



Review

# Catalysis and Downsizing in Mg-Based Hydrogen Storage Materials

Jianding Li <sup>1,\*</sup>, Bo Li <sup>1</sup>, Huaiyu Shao <sup>1,\*</sup> , Wei Li <sup>2</sup> and Huaijun Lin <sup>2,\*</sup> 

<sup>1</sup> Institute of Applied Physics and Materials Engineering (IAPME), University of Macau, Macau SAR, China; ljd982972596@163.com (J.L.); lib@mail.sustc.edu.cn (B.L.)

<sup>2</sup> Institute of Advanced Wear & Corrosion Resistance and Functional Materials, Jinan University, Guangzhou 510632, China; liweijnu@126.com

\* Correspondence: hshao@umac.mo (H.S.); hjlin@jnu.edu.cn (H.L.)

Received: 31 January 2018; Accepted: 15 February 2018; Published: 23 February 2018

**Abstract:** Magnesium (Mg)-based materials are promising candidates for hydrogen storage due to the low cost, high hydrogen storage capacity and abundant resources of magnesium for the realization of a hydrogen society. However, the sluggish kinetics and strong stability of the metal-hydrogen bonding of Mg-based materials hinder their application, especially for onboard storage. Many researchers are devoted to overcoming these challenges by numerous methods. Here, this review summarizes some advances in the development of Mg-based hydrogen storage materials related to downsizing and catalysis. In particular, the focus is on how downsizing and catalysts affect the hydrogen storage capacity, kinetics and thermodynamics of Mg-based hydrogen storage materials. Finally, the future development and applications of Mg-based hydrogen storage materials is discussed.

**Keywords:** magnesium; catalysis; downsizing; thermodynamics; kinetics

## 1. Introduction

In the past few decades, hydrogen energy has drawn a great deal of attention with the increase in the energy crisis and environmental pollution due to massive and long-term depletion of fossil fuels. Thus, it is of great importance to develop clean and renewable energy as a substitute for fossil fuels [1]. Hydrogen is considered to be a promising alternative energy carrier for future the because of its outstanding advantages, such as it has a wide variety of sources (it is the most abundant element in the universe), high energy density and environmentally friendly emissions (no CO<sub>2</sub> emissions, just H<sub>2</sub>O) [2–4]. Hydrogen energy systems include production, storage, transportation, utilization of hydrogen, etc. Among these, hydrogen storage is a key technology limiting the commercialization of hydrogen energy. There are three types of methods to store hydrogen, which include compressed gas storage, low-temperature liquid storage and solid-state storage [2,5–8]. However, poor volumetric hydrogen density (4.4 MJ/L), high cost of the tank and safety issues have limited the wide application of compressed hydrogen storage technology. Although liquid hydrogen storage (8.4 MJ/L) has almost twice the energy content of hydrogen, hydrogen liquidation requires extremely low temperatures (−252 °C) to achieve enough hydrogen capacity, which greatly increases the cost [9,10]. In contrast, solid-state hydrogen storage is thought to be a promising method due to its relatively high energy density, low cost of containment and safety guarantee. Storage of hydrogen in solid-state materials is deemed to be an efficient and safe method. Therefore, one of the hot topics of research is the development of high capacity hydrogen materials and technology. Due to its low price (ca. 3 USD/kg), great abundance and high theoretical hydrogenation capacity (7.7 wt %), magnesium and its alloys are thought to be promising candidates for hydrogen storage materials [11–13]. Unfortunately, the problem of high bonding energy Mg–H causes its high dehydrogenation temperature and poor dehydrogenation

kinetics, which have seriously hindered its commercial applications [14–16]. In order to improve the hydrogen storage performance of Mg-based materials, numerous efforts have been made to enhance the kinetics and destabilize the magnesium hydride, including downsizing, catalysis, etc. So, in this paper, we present some progress in the development of the Mg-based hydrogen storage materials related to the downsizing and catalysts and focus on how downsizing and catalysts could affect the hydrogen storage capacity, kinetics and thermodynamics of hydrogen storage materials.

## 2. Downsizing

In order to realize the downsizing of Mg-based materials, many nanotechnologies have been tried to synthesize these materials with a smaller grain size, including the hydrogen plasma metal reaction technique, high pressure reaction ball milling, thin film synthesis, catalyzed chemical solution synthesis, etc. Figure 1, shows that the kinetics can be expressed by the activation energy of reaction ( $E_a$ ) while the thermodynamics can be characterized by the formation enthalpy ( $\Delta H$ ) and entropy ( $\Delta S$ ) of metal hydride [17]. Here, we will focus on how the  $E_a$ ,  $\Delta H$  and  $\Delta S$  changes when the size is decreased to nanoscales.

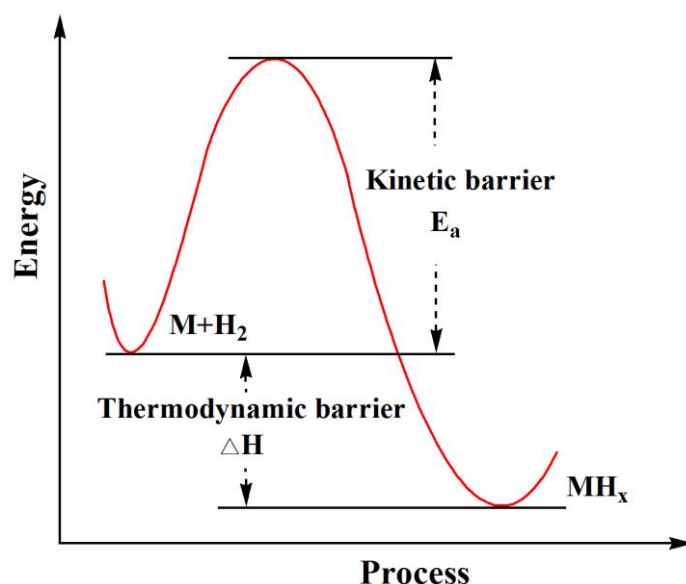


**Figure 1.** Schematic illustration of thermodynamic and kinetic barrier for de-/hydriding reactions of metal hydrides. Adapted with permission from [17], Copyright Elsevier, 2016.

### 2.1. Effect of Downsizing on Desorption Thermodynamics

There is a great deal of debate about the effect of downsizing on desorption thermodynamics. Whether downsizing influences the desorption thermodynamics is controversial. Thus, we examine the relationship between the desorption enthalpy and the diameter of different materials.

Some researchers consider that thermodynamic destabilization is enhanced by reducing the particle sizes of  $MgH_2$ . Theoretical calculations have predicted the size effect of magnesium-base materials. It has been suggested that the thermodynamics properties will be significantly improved and that the adsorption temperature subsequently reduces when the particle size decreases. Chen et al. [18] investigated the hydrogen storage of magnesium nanowires using the calculation of first-principles density functional theory. Results suggested that reducing the size of magnesium and magnesium nanowires could lead to a thermodynamic destabilization. The calculated desorption enthalpy for  $A2\_MgH_2$  ( $\Phi 0.85$  nm) was 34.54 kJ/mol  $H_2$ , which is lower than that of  $A3\_MgH_2$  with a larger diameter of 1.24 nm (61.86 kJ/mol  $H_2$ ). Furthermore, the desorption temperature for  $A2\_MgH_2$  nanowire is 264.25 K, which is close to ambient temperature.

De Jong et al. [19] used ab initio Hartree-Fock and density functional theory calculations to study the size effect on desorption thermodynamics of magnesium and magnesium hydride. They discovered that the downsizing of  $\text{MgH}_2$  and Mg structures had lower desorption energy originating from the change in lattice energy. It was also found that hydrogen desorption energy dramatically decreases when the crystallite size is smaller than  $\sim 1.3$  nm. For example, the desorption enthalpy for the  $\text{MgH}_2$  cluster of 0.9 nm is 63 kJ/mol  $\text{H}_2$  and the desorption temperature is only 473 K. In summary, it is clearly seen that magnesium hydride will destabilize significantly, due to the weakened bonding of H with magnesium, when the particle size is less than 2 nm. The above results of the theoretical calculations showed that reducing particle size to less than 2 nm can greatly enhance thermodynamic destabilization.

Besides the proven effect of nanosizing on desorption thermodynamics by computational results, some experimental results also verify the increase in thermodynamic destabilization when the grain size of Mg/ $\text{MgH}_2$  is reduced to a few nanometers. Fang et al. [20] synthesized a nanostructured  $\text{MgH}_2\text{-0.1TiH}_2$  material by milling the mixture of  $\text{MgH}_2$  and  $\text{TiH}_2$  for 4 h at room temperature under 13.8 MPa hydrogen pressure.  $\text{MgH}_2\text{-0.1TiH}_2$  in the size range of 5~10 nm was obtained. Results also indicated that the nanostructured  $\text{MgH}_2\text{-0.1TiH}_2$  (68 kJ/mol  $\text{H}_2$ ) had lower desorption enthalpy than that of  $\text{MgH}_2$  (75 kJ/mol  $\text{H}_2$ ). However, in a similar experiment, Shao et al. reported that after milling under 30 MPa hydrogen, the obtained nanostructured  $\text{MgH}_2\text{-0.1TiH}_2$  showed greatly enhanced kinetics, but the desorption thermodynamics was not changed [21]. Here it should be noted, that when downsizing and additive introduction are employed together in Mg-based materials, it is challenging to distinguish the specific enhancement mechanisms.

Li et al. [22] fabricated magnesium nanowires with a diameter in the range of 30~170 nm by using a vapor-transport approach and found that the desorption enthalpies for the magnesium nanowire of 30~50 nm, magnesium nanowire of 80~100 nm and rod-like magnesium particles of 150~170 nm were 65.3, 65.9 and 67.2 kJ/mol  $\text{H}_2$ , respectively, which are all smaller than that of bulk  $\text{MgH}_2$  (75 kJ/mol  $\text{H}_2$ ). These experimental findings were in agreement with computational results to some extent.

Although there are many positive results reported in the literature, some researchers have pointed out that downsizing magnesium materials might not change the desorption thermodynamic properties [23]. Theoretically, Goddard et al. [24] carried out simulations focused particularly on the size effect of  $\text{MgH}_2$  in the process of hydrogen absorption/desorption. The results revealed that a steep increase in formation heat and a decrease in structural stability as the particle size decreases below 1.0 nm. Moreover, when the size of the nanoparticle is beyond 2 nm, the difference between the nanoparticle and the bulk can be ignored. The results theoretically explain why magnesium nanoparticles with a size of about 100 nm exhibit insignificant change in thermochemical properties. Other experimental findings also confirm that magnesium hydride particles with a diameter of approximately 100 nm show small thermodynamic change when theoretic simulation is carried out.

Vajo et al. [25] prepared a nanostructured magnesium hydride with a diameter of about 100 nm which was incorporated in a mesoporous carbon aerogel. Results revealed that no significant desorption thermodynamic change occurred in the magnesium hydride-filled nickel decorated aerogel. Similarly, the desorption enthalpies for the magnesium hydride incorporated into copper and magnesium hydride-filled aerogel without wetting layers did not change.

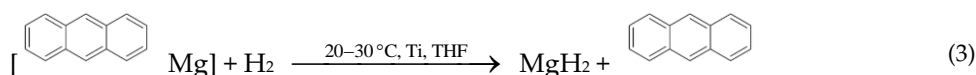
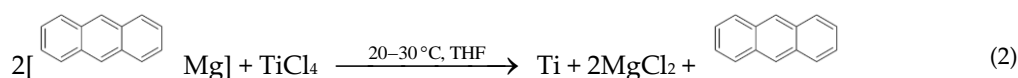
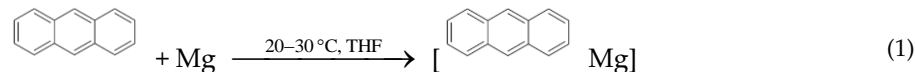
Lin et al. [26] synthesized  $\text{MgH}_2$ -based hydride composites with a crystallite size of about 20 nm from amorphous  $\text{Mg}_{80}\text{Ce}_{10}\text{Ni}_{10}$  alloys via melt-spinning and hydrogenation. It was found that the desorption enthalpy and entropy of  $\text{MgH}_2$  were  $-77.9 \pm 0.3$  kJ/mol and  $139.8 \pm 0.5$  J/mol, respectively. The thermodynamics data was the same as that of  $\text{MgH}_2$  with a size of about 100 nm in their previous study, indicating that the thermodynamics for  $\text{MgH}_2$  desorption are not altered when  $\text{MgH}_2$  particles are in the range of 20~100 nm.

Shao et al. [27] obtained magnesium ultrafine particles (magnesium UFPs) with an average size of about 300 nm via hydrogen plasma-metal reaction and found that the as-prepared magnesium UFPs showed excellent hydrogen storage performance. The hydrogen absorption content for the Mg

UFPs without additives reached 7.59 wt % at 673 K in a few minutes, which was the highest of the studied temperatures. It could be concluded that the value of desorption enthalpy did not change a lot compared to other reported results. The nanostructured  $\text{Mg}_2\text{Ni}$  with diameters in the range of 30–50 nm via hydrogen plasma-metal reaction in 40 bar hydrogen at 623 K reported by Shao et al. [28] also indicated that the formation enthalpy for  $\text{Mg}_2\text{NiH}_4$  is  $-66.32$  kJ/mol  $\text{H}_2$ . This is in agreement with the reported results, which suggests that the enthalpy values are almost the same.

As mentioned above, Shao et al. [21] fabricated the nanostructured  $\text{MgH}_2/0.1\text{TiH}_2$  via ball-milling a mixture of magnesium and titanium powders under an initial hydrogen pressure of 30 MPa. The average crystallite size of the powder after milling was 5 nm. Both the nanostructure and the catalyst  $\text{TiH}_2$  may contribute greatly to the improvement in kinetics, but they do not change the desorption thermodynamics. The desorption enthalpy for as-prepared material and commercial magnesium are 77.4 kJ/mol  $\text{H}_2$  and 78.5 kJ/mol  $\text{H}_2$ , respectively. This agrees with the reported data, and suggests that the enthalpy values do not fluctuate much.

Shao et al. [29] also synthesized the nanocrystalline Ti-catalyzed magnesium hydride in the range of 5–100 nm, by a homogeneously catalyzed synthesis method. Equations (1)–(3) show a typical procedure for fabricating Ti-catalyzed magnesium hydride. It was found that both the Ti catalyst and crystalline structure may contribute to the improvement in hydrogen storage kinetics. The Ti-catalyzed  $\text{MgH}_2$  can absorb hydrogen under a temperature of 130 °C, and its hydrogen absorption rate at 300 °C is 40 times higher than that of commercial  $\text{MgH}_2$  (Figure 2). In the desorption process, the equilibrium pressures for the nano- $\text{MgH}_2^*$  are 0.0385, 0.0585 and 0.1362 MPa at 258, 272 and 299 °C, respectively. The desorption enthalpy and entropy values of the nano- $\text{MgH}_2^*$  are 77.7 kJ/mol  $\text{H}_2$  and 138.3 J/Kmol  $\text{H}_2$ , respectively, which implies that thermodynamic properties do not change with nanostructure and catalyst. Thus, it may be concluded that materials with a diameter above 5 nm do not change desorption thermodynamics.



In order to more clearly understand the relationship between the thermodynamic properties and the size of particles, we tried to identify as many Mg- $\text{MgH}_2$  systems for hydrogen storage as possible. The temperature range, van't Hoff equations, enthalpy and entropy change values of different Mg- $\text{MgH}_2$  systems are listed in Table 1. Figure 3 shows the van't Hoff plots of desorption reaction for different Mg- $\text{MgH}_2$  systems. In Table 1, it can be seen that commercial magnesium hydride has a  $\Delta H$  of 78.5 kJ/mol  $\text{H}_2$  and  $\Delta S$  of 140 J/Kmol  $\text{H}_2$ . When we compare these values to those reported by other systems for  $\text{MgH}_2/0.1\text{TiH}_2$ , for example, by ball milling ( $\Delta H$  of 77.4 kJ/mol  $\text{H}_2$  and  $\Delta S$  of 137.5 J/Kmol  $\text{H}_2$ ), magnesium ultrafine particles ( $\Delta H$  of 79.8 kJ/mol  $\text{H}_2$  and  $\Delta S$  of 140.8 J/Kmol  $\text{H}_2$ ), magnesium hydride (enthalpy change of  $\Delta H$  kJ/mol  $\text{H}_2$  and  $\Delta S$  of 135.8 J/Kmol  $\text{H}_2$ ), and Ti-catalyzed  $\text{MgH}_2$  ( $\Delta H$  of 77.5 kJ/mol  $\text{H}_2$  and  $\Delta S$  of 138.3 J/Kmol  $\text{H}_2$ ), we can further conclude that there is no apparent change of thermodynamic properties in desorption reactions when downsizing the diameter from 5 to 300 nm. This is also in agreement with Wagemans et al. [19] findings in their quantum chemical study.

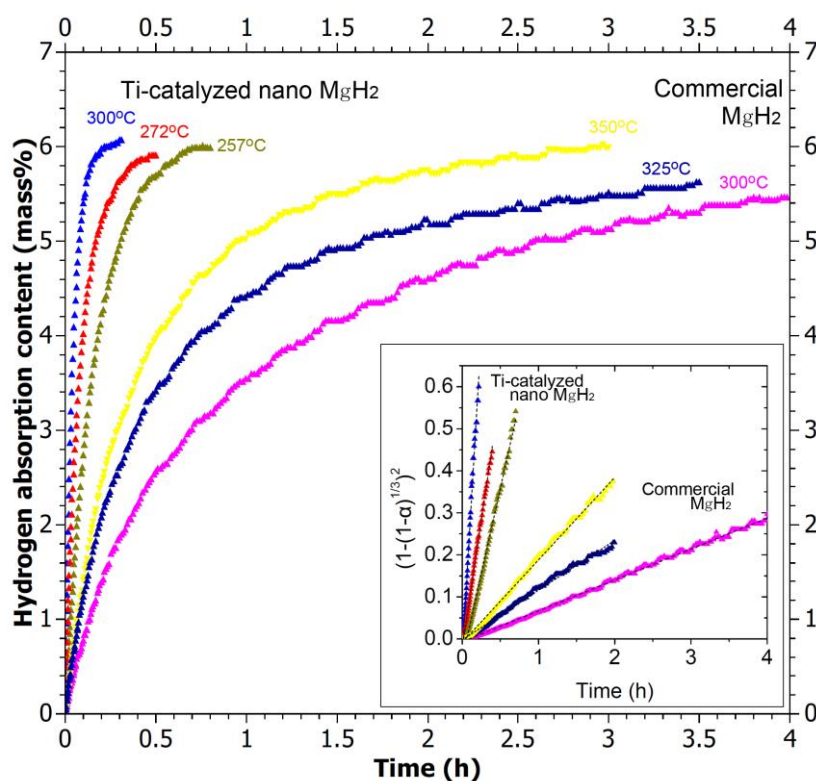


**Figure 2.** Hydrogen re-absorption curves of Ti-catalyzed  $MgH_2$  nanocrystalline sample and commercial  $MgH_2$  sample (Alfa Aesar) at different temperatures in 1 MPa hydrogen after complete desorption (inset: absorption curves simulated by Jander diffusion equation). Adapted with permission from [29], Copyright IOP, 2011.

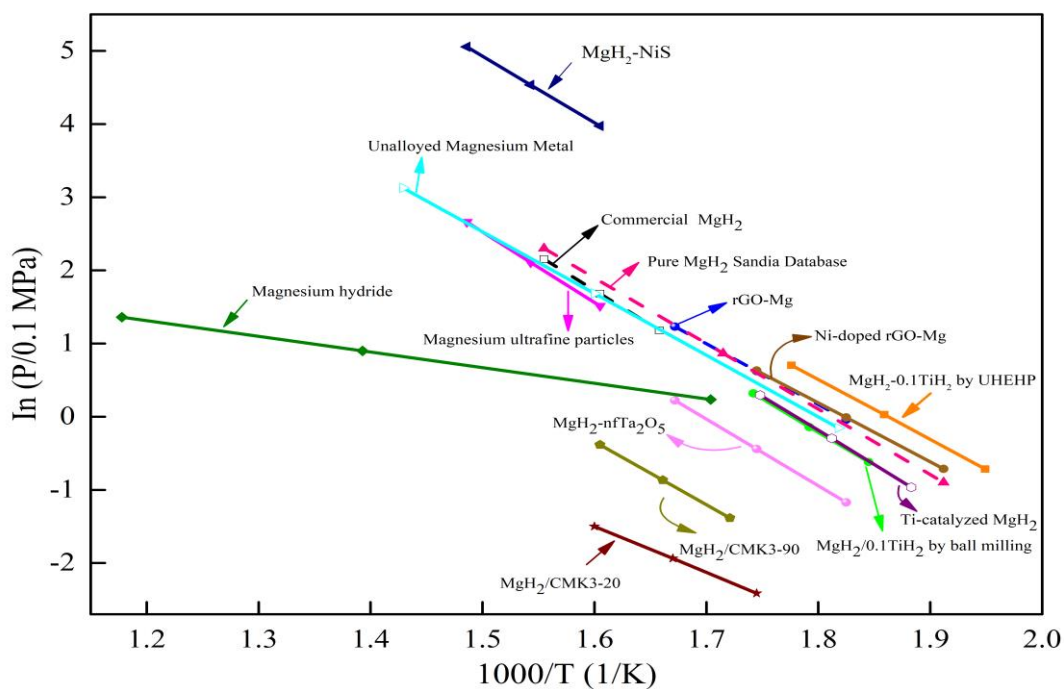


**Figure 3.** The van't Hoff plots of the desorption reaction for various Mg- $MgH_2$  systems.

Based on the above-mentioned results and considering the error margins of the experiments, it can be concluded that the thermodynamic properties do not change with nanostructure in the diameter range of 5–300 nm. According to the Gibbs free energy of the hydriding reaction equation,  $\Delta G = RT \ln P_{\text{eq}}/P_{\text{H}_2}$ , it is found that the hydriding reaction is thermodynamically favored when  $P_{\text{H}_2} > P_{\text{eq}}$ ,  $\Delta G < 0$  [30]. Since,  $P_{\text{eq}}$  depends upon the temperature, selecting a different temperature range would affect the  $P_{\text{eq}}$  and then the thermodynamics, which may not be affected by the downsizing. Recently, Shao et al. [31] found that the reaction pathway of the decomposition process is changed from two steps to three steps at 633 K, which indicates that we can indirectly change the thermodynamics properties by controlling the reaction pathway through catalysis design.

**Table 1.** The temperature range, van't Hoff equations, enthalpy and entropy change values of different Mg-based systems.

System	Temperature Range (°C)	Van't Hoff Equation	$\Delta H$ (kJ/mol H <sub>2</sub> )	$\Delta S$ J/(K mol H <sub>2</sub> )	Reference
MgH <sub>2</sub> -0.1TiH <sub>2</sub> by UHEHP	240–290	$\log P(\text{bar}) = -3560.6/T + 6.6302$	68.2	127	[20]
MgH <sub>2</sub> /0.1TiH <sub>2</sub> by ball milling	269–301	$\ln(P/0.1 \text{ MPa}) = -9308.8/T + 16.539$	77.4	137.5	[21]
Commercial MgH <sub>2</sub>	330–370	$\ln(P/0.1 \text{ MPa}) = -9445.1/T + 16.844$	78.5	140	
Magnesium Ultrafine Particles	350–400	$\ln(P/\text{bar}) = -9604/T + 16.93$	79.8	140.8	[27]
Magnesium hydride	314–576	$\ln f_{\text{H}_2} = -2139.2/T + 3.88$	73.1	135.8	[32]
MgH <sub>2</sub> -NiS	350–400	$\ln P = -9061.7/T + 18.5192$	75.34	153.97	[33]
Unalloyed Magnesium Metal	277–427	$\ln(P/0.1 \text{ MPa}) = -8419.5/T + 15.155$	70	126	[34]
Ti-catalyzed MgH <sub>2</sub>	258–299	$\ln(P/0.1 \text{ MPa}) = -9345.7/T + 16.635$	77.7	138.3	[29]
MgH <sub>2</sub> /CMK3-20	300–350	$\ln(P/0.1 \text{ MPa}) = -6300.2/T + 8.580$	52.38	71.33	
MgH <sub>2</sub> /CMK3-90	308–350	$\ln(P/0.1 \text{ MPa}) = -8620.4/T + 13.453$	71.67	111.85	[35]
MgH <sub>2</sub> -n/Ta <sub>2</sub> O <sub>5</sub>	275–325	$\ln(P/0.1 \text{ MPa}) = -9141.2/T + 15.510$	76	129	[36]
rGO-Mg	275–325	$\ln(P/0.1 \text{ MPa}) = -8347.4/T + 15.191$	69.4	126.3	
Ni-doped rGO-Mg	250–300	$\ln(P/0.1 \text{ MPa}) = -8046.7/T + 14.674$	66.9	122	[37]
Pure MgH <sub>2</sub>	250–370	$\log(P/0.1 \text{ MPa}) = -3893.8/T + 7.055$	74.6	135.1	Sandia National Lab database

## 2.2. Effect of Downsizing on Kinetics

Kinetics is another issue that must be addressed before the studied hydrogen storage materials are widely used. It is known that fast kinetics shorten the time required to absorb/release hydrogen. Therefore, good kinetics is essential for hydrogen storage. It is reported that reducing the size of hydrogen storage materials could lead to a remarkable change in hydrogen absorption/desorption kinetics [12,38–41]. It is well proven that small particles of hydrides have an influence on hydrogen absorption/desorption kinetic properties, mainly due to shortened hydrogen diffusion and dissociation pathways, and enlarged surface free energy when the size decreases to below a few nanometers [42,43]. Numerous methods are applied to synthesize the hydrogen storage nanostructured materials, including ball milling, the hydrogen plasma metal reaction, nano-confinement, thin film synthesis, and catalyzed solution synthesis. Many experiments show that absorption and desorption kinetics can be enhanced by simply decreasing the size of the materials.

Shao et al. [44,45] synthesized six different magnesium based materials (325 mesh Mg, single crystal Mg, Mg nanoparticles, nanocrystalline Mg<sub>50</sub>Co<sub>50</sub> BCC alloy and Mg thin film samples) to investigate their hydrogen absorption kinetics. Figure 4, shows that the grain sizes are in the range of 40–50  $\mu\text{m}$  for 325 mesh Mg sample particles, and 100–700 nm for the Mg nanoparticles. The BCC Mg<sub>50</sub>Co<sub>50</sub> alloy shows a particle size of about 1 to 3  $\mu\text{m}$  with a few nanometers in crystallite size. For the 84 nm-thick Mg thin film capped by 10 nm Pd layer, the crystallite size is around 50–100 nm. Hydrogen absorption kinetics of the as-prepared materials have been obtained and it has been concluded that the absorption kinetics are significantly in nanoscale and micrometer scale material. For example, Mg nanoparticles have better absorption kinetics than 325 mesh Mg due to

their smaller grain size. As a result, there is more chance and more surface area available for hydrogen to react with Mg materials. Besides, the hydrogen diffusion distance decreases in Mg nanoparticles. In addition, the nanostructured  $Mg_{50}Co_{50}$  BCC alloy could absorb hydrogen at near room temperature (303 K) under 3.3 MPa hydrogen, and even at 258 K, achieving a hydrogen capacity of up to 2.65 wt % under hydrogen pressure of 8 MPa (Figure 5). This is the lowest absorption temperature reported so far for Mg-based materials. On the contrary, the single crystal Mg with a millimeter scale does not obtain any hydrogen absorption ability below 573 K. Thus, downsizing the diameter can enhance the hydrogen absorption/desorption kinetics properties.

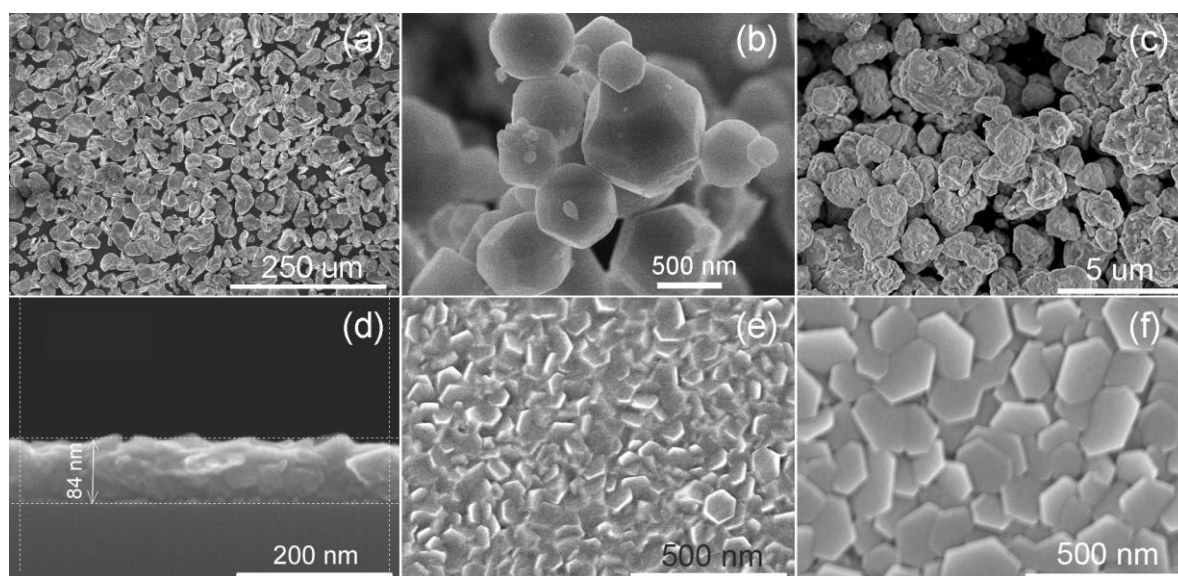


**Figure 4.** SEM images of (a) 325 mesh Mg, (b) Mg nanoparticle sample, (c) milled  $Mg_{50}Co_{50}$  bcc alloy, (d) cross-section observation of Mg thin film without Pd layer, (e) top view of Mg thin film without Pd layer and (f) top view of Pd capped Mg thin film. Adapted with permission from [44], Copyright Elsevier, 2014.

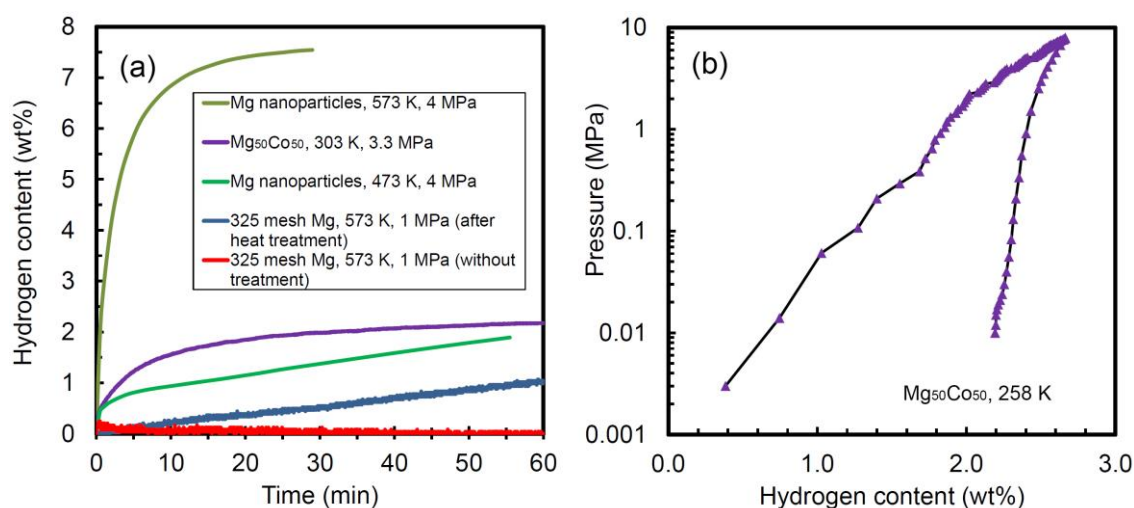


**Figure 5.** (a) Hydrogen absorption curves of Mg-based samples in different hydrogen atmosphere and temperature conditions and (b) pressure-composition isotherm at 258 K of the ball milled  $Mg_{50}Co_{50}$  BCC structure alloy. Adapted with permission from [44], Copyright Elsevier, 2014.

### 3. Catalysis

The natural kinetics properties of pure magnesium are very slow, therefore high pressure and high temperatures are required to improve the kinetics. When it comes to thermodynamics, magnesium hydride needs even higher temperature to desorb hydrogen [30,46,47]. In addition, the activation process of hydrogenation and dehydrogenation requires high temperatures of approximately 350 °C under hydrogen pressure to 70 atm without any additives [48]. In order to accelerate the kinetics of hydrogen absorption and desorption, numerous studies have been done to improve these performances. Catalytic additives (like transition metal, metal oxide, halides, etc.) are combined with Mg-based materials to enhance the kinetics of absorption and desorption.

#### 3.1. The Doping of Transition Metals

The doping of transition metals can be an effective way to enhance the kinetics of hydrogenation/dehydrogenation. Many researchers have doped different transition metals to improve the kinetics. Hanada et al. [49] prepared magnesium hydride doped with different 3d-transition metals (Fe, Co., Ni, and Cu) by a mechanical ball milling method, and found that all doped MgH<sub>2</sub> composites showed better hydrogen desorption properties than that of pure MgH<sub>2</sub>. They also reported that the doping of Ni performed best among these doped MgH<sub>2</sub> materials. The superior hydrogen desorption properties of Ni doped MgH<sub>2</sub> are mainly ascribed to the fact that the Mg<sub>2</sub>Ni phase is generated in the boundary between the MgH<sub>2</sub> phase and Ni catalyst after hydrogenation. In addition, the decrease in activation energy for hydrogen desorption after doping by Ni also explains the phenomenon.

Liang et al. [50] fabricated the composites of MgH<sub>2</sub> + 5at%Tm (Tm = Ti, V, Mn, Fe, Ni) to investigate the hydrogen desorption of the mixture. Results showed that all the doped composites presented better absorption kinetics than that of the undoped MgH<sub>2</sub>. Moreover, the catalytic effect of the five metals (Ti, V, Mn, Fe, Ni) is different. The composites containing Ti showed the best absorption kinetics and MgH<sub>2</sub> + 5 at%V exhibited the most rapid desorption kinetics at low temperature among these metal doped composites. In order to further investigate the catalytic effect of vanadium, they ball-milled the mixture of magnesium hydride and 15 wt % vanadium. The enhanced kinetics are attributed to the vanadium hydride working as a hydrogen pump, the specific area, smaller particle size and the introduction of defects [51].

Cui et al. [52] fabricated nanostructured Mg-based materials coated by multi-valence Ti-based catalysts by the reaction of magnesium powder in THF solution with TiCl<sub>3</sub>. It was found that the Mg-Ti with a crystal size of ~10 nm significantly reduced hydrogen absorption and desorption temperatures. The coated magnesium begins to release H<sub>2</sub> at about 175 °C and releases 5 wt % H<sub>2</sub> within 15 min at 250 °C. The dehydrogenation entropy also changes from 130.5 J K<sup>-1</sup> mol<sup>-1</sup> H<sub>2</sub> to 136.1 J K<sup>-1</sup> mol<sup>-1</sup> H<sub>2</sub>. The schematic diagram of the catalytic mechanism is presented in Figure 6. The authors believe that the improvements may originate from the multiple valence Ti acting as the intermediate for electron transfers between Mg<sup>2+</sup> and H<sup>-</sup>, which significantly contributed to better dehydrogenation.

Lu et al. [53] obtained core-shell structured Mg@TM (TM = Co., V) composites via an approach combining the arc plasma method and electroless plating. Results showed that the hydrogen absorption/desorption enthalpies for Mg@Co.@V (−70.02/74.83 kJ/mol H<sub>2</sub>) were both lower than those for the Mg@Co. (73.25/81.47) and Mg@V (−73.91/79.77) samples. In addition, the E<sub>a</sub> value is 73.22 kJ/mol H<sub>2</sub> for Mg@Co., 86.30 kJ/mol H<sub>2</sub> for Mg@V and 67.66 kJ/mol H<sub>2</sub> for Mg@Co.@V, which are all lower than that of the pure magnesium ultrafine powder (118.20 kJ/mol H<sub>2</sub>). These enhancements may be attributed to the core-shell microstructures and catalytic effects of both V and Co.

Zou et al. [54] prepared the Mg-Transition metal (TM)-La (TM = Ti, Fe, Ni) ternary composites via arc plasma evaporation and carefully investigated the hydrogen sorption properties of the as-prepared composites, leading to significantly improvement in the kinetics of hydrogen absorption and reduction in the temperature of hydrogen desorption. The improvement was attributed to catalytic effect of both Mg<sub>2</sub>Ni and La<sub>2</sub>O<sub>3</sub>.



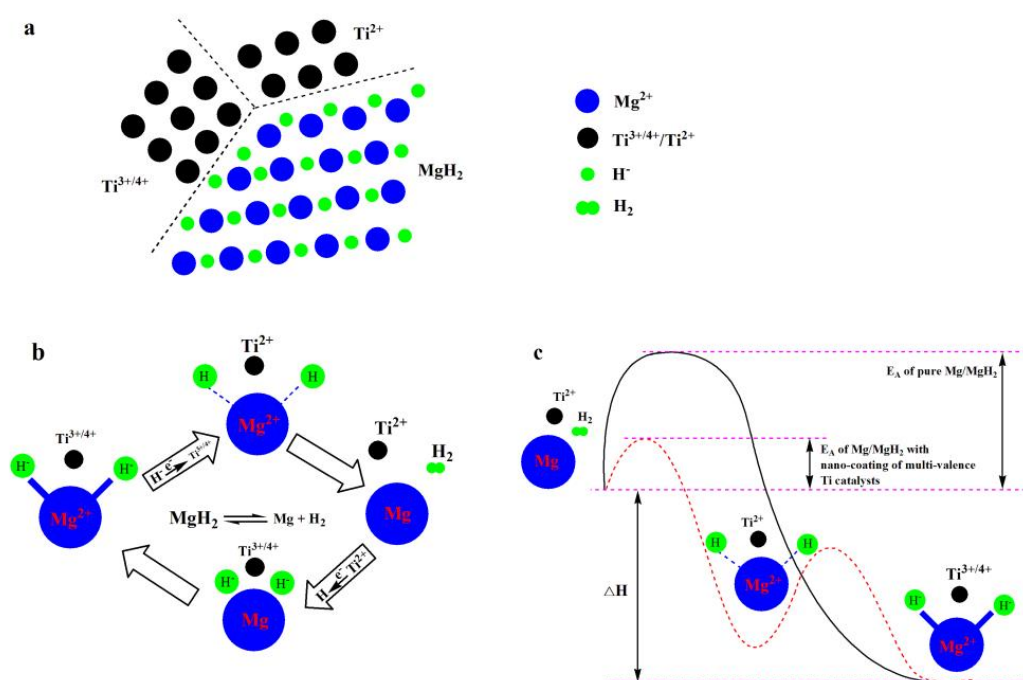


**Figure 6.** (a) Interfaces with high and low valence Ti among  $\text{MgH}_2$ , (b) electron transfer between  $\text{Mg}^{2+}$  and  $\text{H}^-$ , and (c) schematic diagram of catalytic mechanism in de-/hydrogenation of Ti based multi-valence coated  $\text{MgH}_2$ . Adapted with permission from [52], Copyright RSC, 2013.

Magnesium with 10 wt % of metal nanoparticles (Fe, Co., Ni, Cu and Zn) was ball-milled at a rotation of 300 rpm for 4 h under the inert atmosphere of argon by Yu et al. [55]. They confirmed that there was no new phase formation between magnesium hydride and the introduced Fe, Co., Ni metals even after several cycles of hydrogenation/dehydrogenation. In addition, the introduction of metal particles into  $\text{MgH}_2$  resulted in lower hydrogen desorption temperatures than that of pure magnesium hydride. Also the nickel-contained magnesium hydride showed the best result with the lowest desorption temperature centered at 203 °C, among these as-prepared materials. Interestingly, the added Zn and Cu metal act as an inhibitor without catalyst in the hydrogenation process because they do not improve the hydrogen absorption kinetics of  $\text{MgH}_2\text{-10-Zn}^{\text{nano}}$  and  $\text{MgH}_2\text{-10-Cu}^{\text{nano}}$ .

Kuji et al. [56] prepared ternary Mg-Tm-V (Tm = Ni, Co., Cu) alloys by mechanical alloying of powder mixture with a milling time from 5 to 25 h at the rate of 12.3 rev/s. The results showed that the hydrogen storage capacities for  $\text{Mg}_{1.0}\text{Ni}_{1.0}\text{V}_{1.0}$  was 2.3 wt %, which was followed by  $\text{Mg}_{1.0}\text{Co}_{1.0}\text{V}_{1.0}$  (1.44 wt %) and  $\text{Mg}_{1.0}\text{Cu}_{1.0}\text{V}_{1.0}$  (0.95 wt %) alloys at 298 K under the pressure of 3 MPa. In addition, all the as-prepared materials were mechanically alloyed to the BCC structure.

Xie et al. [57] synthesized different amounts of nickel doped magnesium hydrides by ball milling at the rate of 300 rpm for 2 h under 2 bar hydrogen pressure. The results of XRD and electron microscopy indicated that the as-prepared  $\text{MgH}_2 + \text{Ni}$  materials show almost the same particle size. Besides, the obtained  $\text{MgH}_2 + 10 \text{ wt \% Ni}$  desorbed 6.1 wt % hydrogen in 10 min at 523 K under an initial hydrogen pressure of about 0.01 bar, followed by  $\text{MgH}_2 + 25 \text{ wt \% Ni}$ ,  $\text{MgH}_2 + 50 \text{ wt \% Ni}$ ,  $\text{MgH}_2 + 80 \text{ wt \% Ni}$  and  $\text{MgH}_2$ . Xie et al. identify and discuss the four effects of the doping of nickel on the dehydrogenation of  $\text{MgH}_2$  as follows: the decomposition of hydride phase to form magnesium phase, the diffusion of hydrogen atoms, the combination of hydrogen atoms on the surface, and the desorption of hydrogen molecules. They conclude that the introduction of nickel is mainly to accelerate the combination of hydrogen atoms on the surface of  $\text{MgH}_2$ .

The method of melt-spinning was adopted to fabricate the nano-crystalline magnesium-rich magnesium-nickel-yttrium (Mg-Ni-Y) ternary alloys ( $\text{Mg}_{80}\text{Ni}_{10}\text{Y}_{10}$  and  $\text{Mg}_{90}\text{Ni}_5\text{Y}_5$ ) under argon

atmospheres by Kalinichenka et al. [58]. They investigated the crystal structure, crystallization behavior and cyclic hydrogenation/dehydrogenation properties of the as-prepared materials. It was found that both Mg-Ni-Y ternary alloys mainly contain Mg(Ni,Y) nanocrystals with an average size in the range of 5–20 nm embedded in an amorphous matrix. Also, the Mg<sub>80</sub>Ni<sub>10</sub>Y<sub>10</sub> alloy presents higher thermal stability and a faster hydrogenation rate than that of the Mg<sub>90</sub>Ni<sub>5</sub>Y<sub>5</sub> alloy, which may be due to the higher content of yttrium and nickel. In addition, the two activated alloys can absorb almost 5.3 wt % hydrogen at a temperature of 280 °C and under the pressure of 20 bar H<sub>2</sub>.

Cho et al. [37] reported the 3d transition metals (Ti, Cr, Mn, Fe, Co. and Ni) doped magnesium crystals encapsulated by rGO layers by a solution based, one-pot synthesis method. Based on the TEM image of the Ni-doped rGO–Mg nanocomposite, the diameter of magnesium crystals is about 3.56 nm. In Figure 7c, the XRD data shows a clear Mg crystalline structure without oxidation, which is evidence that the Mg is successfully encapsulated by molecular-sieving rGO layers (Figure 7a). It was also found that the dopants, Ni, Cr and Mn show preferable absorption rate when compared with other dopants during the first absorption (Figure 7d). In addition, Ni-doped Mg crystals embedded in rGO layers (Ni-doped rGO–Mg) can absorb 6.5 wt % hydrogen and most absorbed hydrogen of about 90% was completed within 2.5 min at 200 °C. When it comes to desorption, the absorbed hydrogen can completely desorb at 300 °C, of which 90% was dehydrogenated within 4.6 min. In summary, the as-prepared Ni-doped rGO–Mg present excellent hydrogen storage properties owing to the synergistic effect of nanosizing, rGO encapsulation and Ni doping. These three complementary functional materials will provide a novel way to make metal hydride.

Shao et al. [59] ball-milled a mixture of magnesium powder and cobalt powder at the rotation speed of 200 rpm for varying times from 0.5 h to 400 h under 0.1 MPa argon and then investigated the phase, morphology, hydrogen storage properties and mechanisms of nanostructured Mg<sub>50</sub>Co<sub>50</sub> materials. It was found that the particle size reduces within 100 h and is not further changed after ball milling. In addition, the morphologies of magnesium based materials are transformed from the Co. phase with FCC structure, Co. phases with HCP and FCC together, then FCC Co. and partial bcc Mg-Co., into totally Mg<sub>50</sub>Co<sub>50</sub> BCC structure with an average grain size of 1–5 nm. Moreover, the as-prepared Mg<sub>50</sub>Co<sub>50</sub> BCC alloy can absorb hydrogen of 2.67 wt % at 258 K under a hydrogen pressure of 8 MPa and still retain the BCC structure after hydrogenation. It is known that the temperature of 258 K is the lowest reported so far for magnesium based materials to absorb hydrogen. Using the hydrogen plasma metal reaction, some doped magnesium materials (Mg<sub>2</sub>Ni, Mg<sub>2</sub>Co and Mg<sub>2</sub>Cu) with an average particle size in the range of 50–200 nm were obtained and it was found that the doping of Ni, Co. and Cu show excellent hydrogen storage properties [60–62]. The study also reported the nanostructured Mg-Ni system alloys via the mechanical alloying method under 0.1 MPa argon at a rotation speed of 200 rpm for different time periods. Among these as-prepared Mg-Ni system alloys, the Mg<sub>60</sub>Ni<sub>40</sub>, Mg<sub>50</sub>Ni<sub>50</sub>, Mg<sub>40</sub>Ni<sub>60</sub> and Mg<sub>33</sub>Ni<sub>67</sub> alloys with a particle size of 1–3 nm show a BCC structure while the Mg<sub>30</sub>Ni<sub>70</sub> of 5–10 nm show a FCC structure. In addition, the Mg<sub>50</sub>Ni<sub>50</sub> BCC alloy that can absorb 1.85 wt % at 373 K in 7 MPa hydrogen shows the best hydrogen absorption kinetics and absorption efficiency due to the nanostructure and BCC phase when compared with other alloys [63].

Zhang et al. [64] proposed a novel strategy named microencapsulated nano-confinement for the preparation of nearly monodispersed nano-Mg<sub>2</sub>NiH<sub>4</sub> anchored onto a graphene sheet surface via hydriding chemical vapor deposition (HCVD), which is presented in Figure 8. The as-prepared material possesses ultrahigh structural stability and superior desorption kinetics. The MgO coating layer with a thickness of about 3 nm efficiently separates the nanoparticles from each other to prevent aggregation during hydrogen absorption/desorption cycles, leading to excellent thermal and mechanical stability. More interestingly, the MgO layer shows superior gas-selective permeability to prevent further oxidation of Mg<sub>2</sub>NiH<sub>4</sub> meanwhile accessible for hydrogen absorption/desorption (Figure 8b). As a result, an extremely low activation energy of 31.2 kJ mol<sup>−1</sup> for the dehydrogenation reaction is achieved. The study provides alternative insights into designing nano-sized metal hydrides

with both excellent hydrogen storage activity and thermal/mechanical stability, exempting surface modification by agents.

In conclusion, the transition metal added to the magnesium hydride can improve the kinetics of hydrogenation/dehydrogenation, which originates from the introduced catalytic effect, such as the hydrogen pump, the surface/boundary reaction, electron transfer, etc. These ideas provide an insight into making metal hydride.

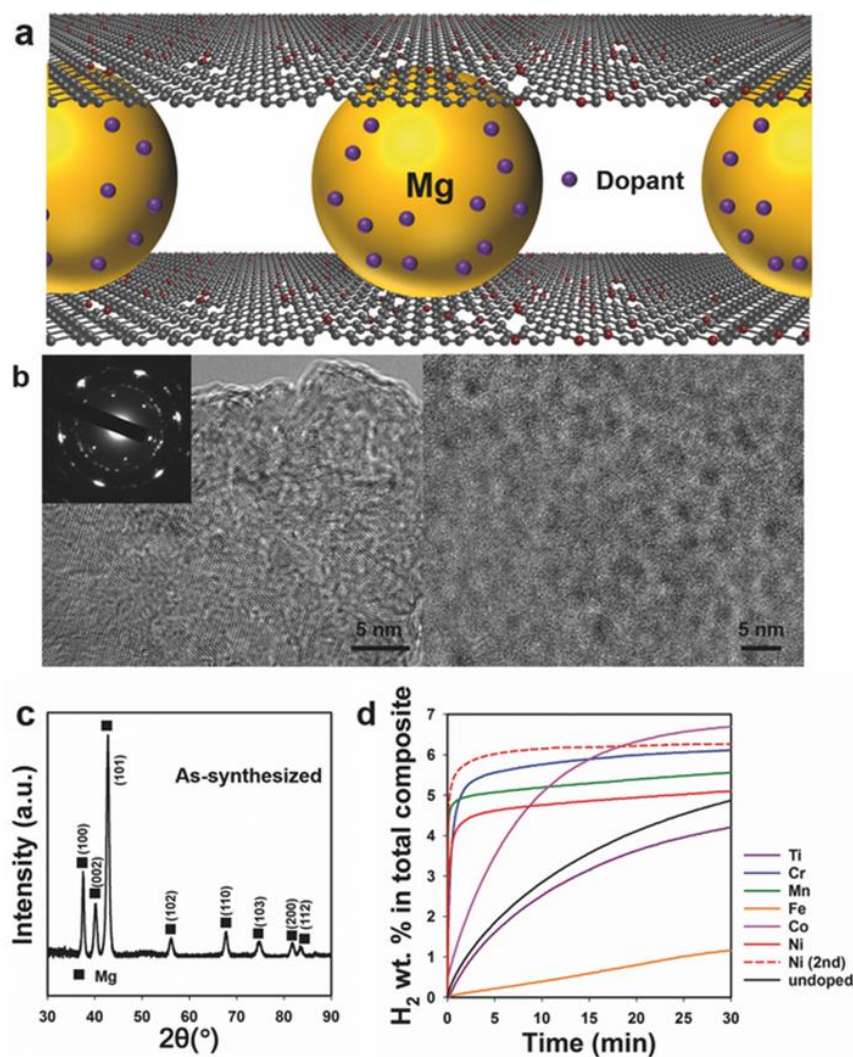


**Figure 7.** (a) Illustration describing Mg nanocrystals encapsulated by reduced graphene oxide layers with transition metal dopants (transition metal doped rGO-Mg); the cartoon is based upon microscopy data and not intended to be an atomistic model. (b) Transmission electron microscope (TEM) images of the Ni-doped rGO-Mg. The diffraction pattern from TEM images is shown in the inset which indicate the crystalline lattice of Mg (010), (002), (100), and graphene (100). (c) X-ray diffraction pattern of as-synthesized transition metal doped rGO-Mg composite; well-defined Mg crystalline structures were observed for all transition metal doped rGO-Mg composites regardless of the specific dopant, and a representative pattern is shown for Ni-doped rGO-Mg. (d) Hydrogen absorption behaviors of a series of 3d transition metal doped rGO-Mg composites at 15 bar of H<sub>2</sub> and 200 °C in comparison with undoped rGO-Mg; red solid and dashed line represent the absorption of the first and the second hydrogen sorption cycles for Ni-doped rGO-Mg, respectively. Adapted with permission from [37], Copyright Wiley, 2017.

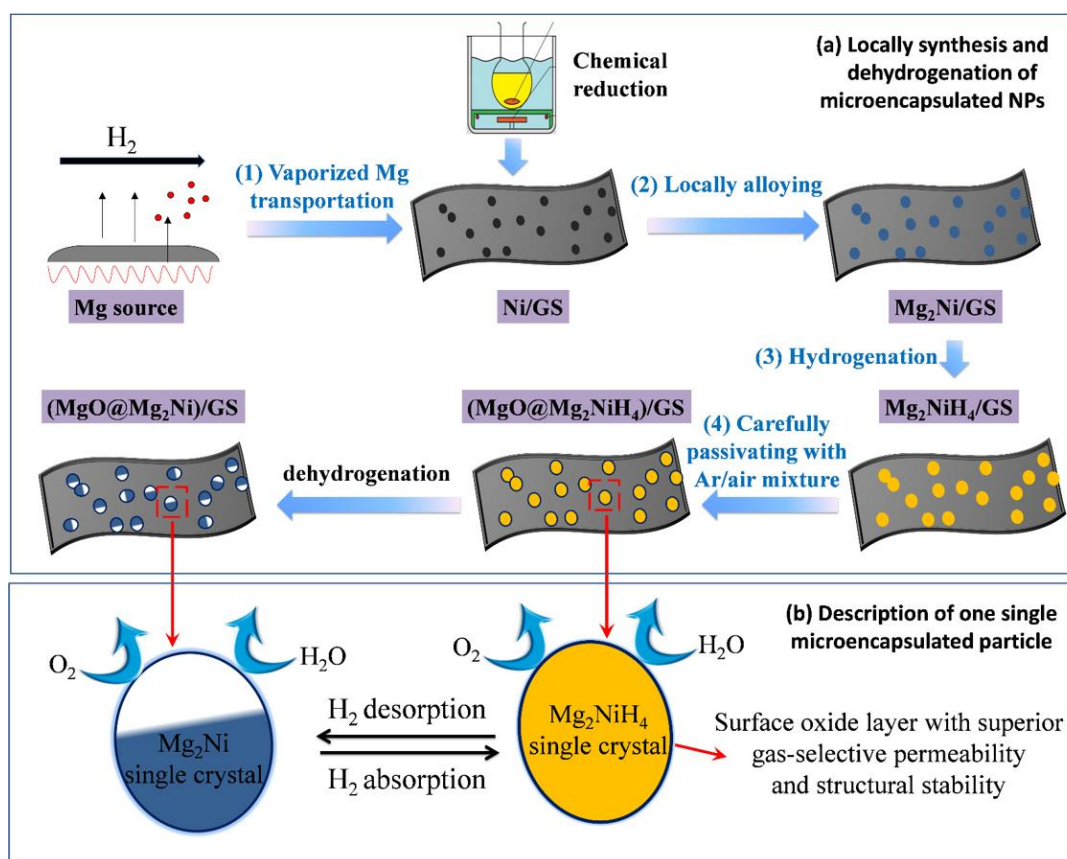


**Figure 8.** Schematic of (a) the local synthesis of monodispersed  $\text{Mg}_2\text{NiH}_4$  nanoparticles locally derived from Ni/GS by HCVD and the structural evaluation after hydrogen desorption. Four steps are involved in the HCVD synthesis: (1) under  $\text{H}_2$  atmosphere, gasified Mg transports to the Ni/GS substrate; (2) the Ni dopants act as positive cores to attract gaseous Mg atoms, and the alloying reaction between them locally generates monodispersed  $\text{Mg}_2\text{Ni}$  NPs on the GS surface; (3)  $\text{Mg}_2\text{Ni}$  absorbs  $\text{H}_2$  and transforms to  $\text{Mg}_2\text{NiH}_4$ ; (4) careful in situ passivation of the NPs to form an MgO coating with a thickness of  $\sim 3$  nm occurs during the cooling process. (b) Detailed description of a single microencapsulated particle. A “semi-hollow” structure is formed upon hydrogen desorption. Adapted with permission from [64], Copyright Wiley, 2017.

### 3.2. Introduction of Metal Oxides

Metal oxides are also valid catalysts to improve the absorption/desorption kinetics of  $\text{MgH}_2$ . Metal oxides ( $\text{Sc}_2\text{O}_3$ ,  $\text{TiO}_2$ ,  $\text{V}_2\text{O}_5$ ,  $\text{Cr}_2\text{O}_3$ ,  $\text{Mn}_2\text{O}_3$ ,  $\text{Fe}_3\text{O}_4$ ,  $\text{CuO}$ ,  $\text{Al}_2\text{O}_3$  and  $\text{SiO}_2$ ) were employed to enhance the hydrogen absorption/desorption kinetics by Oelerich et al. [65]. The initial magnesium hydride was pre-milled for 20 h and then a further 100 h after adding the different metal oxides. Results showed that the addition of metal oxides can lead to a notable enhancement of both absorption and desorption kinetics. Furthermore, among these metal oxides, the  $\text{MgH}_2 + 5$  mol%  $\text{Cr}_2\text{O}_3$  composite obtained the fastest hydrogen absorption as it achieved a capacity of 4.7 wt % within 2 min at  $300^\circ\text{C}$ , while the additives of  $\text{V}_2\text{O}_5$  and  $\text{Fe}_3\text{O}_4$  showed the most rapid desorption of hydrogen. The excellent kinetics may originate from the local electronic structure of the catalysts and a very high defect density introduced by high energy ball milling.

Barkhordarian and collaborators reported several metal oxide catalysts ( $\text{Nb}_2\text{O}_5$ ,  $\text{Fe}_3\text{O}_4$ , et al.) doped  $\text{MgH}_2$ . The  $\text{Nb}_2\text{O}_5$  doped sample presented the fastest hydrogen sorption kinetics among these metal oxides [66]. 6.9 wt % of hydrogen was absorbed within 60 s and the absorbed 6.9 wt % of hydrogen was fully desorbed in only 140 s. The results of the desorption rate for different

metal oxides are listed in Figure 9. It is clearly seen that the  $\text{Nb}_2\text{O}_5$  dopant possessed the fastest desorption rate compared with that of other dopants, yielding a desorption rate of 0.011 wt %/s. It is suggested that metals with multiple valences and the catalytic effect of electronic exchange reacting with hydrogen molecules are able to accelerate the gas-solid reaction. Similar findings also were reported by Ichikawa et al. [67]. In the literature, the effect of adding 1 mol% niobium oxide into the  $\text{MgH}_2$  system by ball-milling for 20 h at 400 rpm was investigated. It was also found that the  $\text{MgH}_2 + 1 \text{ mol\% Nb}_2\text{O}_5$  quickly absorbs hydrogen at ambient temperature even when the hydrogen pressure is lower than 0.1 MPa. At 150 and 250 °C, more than 5.0 wt % hydrogen gas is absorbed within 30 s and its final capacity reached 5.7 wt %. We can see that the amount of additive  $\text{Nb}_2\text{O}_5$  is small. So, Aguey-Zinsou et al. [68] prepared magnesium hydride doped by a large amount of  $\text{Nb}_2\text{O}_5$  (17 wt %). They found that magnesium hydride milled for 200 h has faster hydrogen absorption-desorption kinetics than that for 2 h and magnesium hydride doped by  $\text{Nb}_2\text{O}_5$  is further improved. They considered that the further enhanced kinetics for magnesium doped by  $\text{Nb}_2\text{O}_5$  can be ascribed to the effect of  $\text{Nb}_2\text{O}_5$  which acts as a lubricant, dispersing and cracking agent. Conceição et al. [69] also investigated the hydrogen storage properties of  $\text{Nb}_2\text{O}_5$  combined with magnesium hydride by ball-milling the mixture at the rate of 300 rpm for 24 h under  $\text{H}_2$ . They found that the  $\text{MgH}_2 + 5 \text{ wt\% synthesized-Nb}_2\text{O}_5$  can absorb 5.2 wt % of hydrogen within 1.3 min and desorb almost 6.0 wt % in 5.8 min at the temperature of 300 °C, which are the best results among the as-prepared materials. In addition, they point out that the surface area and the amount of  $\text{Nb}_2\text{O}_5$  greatly affect the hydrogen storage properties. It is easy to conclude that the additive  $\text{Nb}_2\text{O}_5$  may contribute to superior enhanced absorption/desorption kinetics in Mg-based materials.

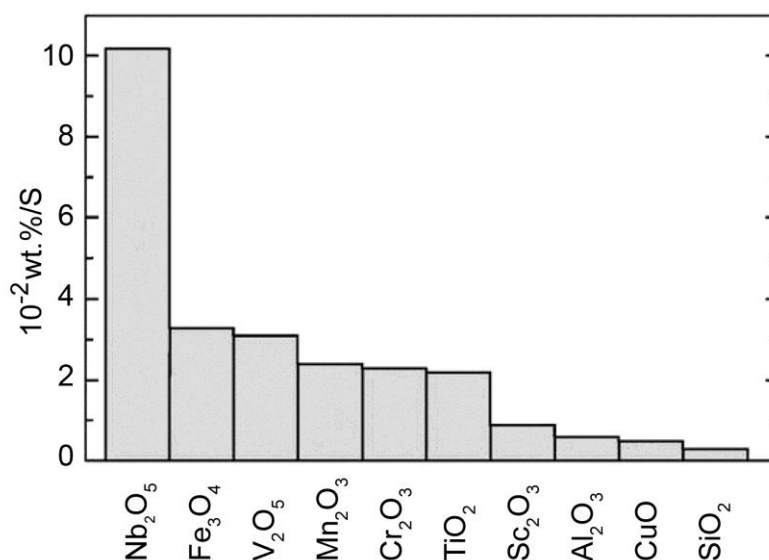


**Figure 9.** Comparison of the desorption rates of  $\text{MgH}_2$  with different metal oxide catalyst additions at 300 °C into vacuum. Adapted with permission from [66], Copyright Elsevier, 2003.

Kumar et al. [36] ball-milled the mixture of magnesium hydride and 5 wt % nano-flakes of  $\text{Ta}_2\text{O}_5$  ( $\text{nfTa}_2\text{O}_5$ ) for 2 h to investigate the effect of the additive on kinetics and thermodynamics of absorption and desorption. Results showed that the  $\text{MgH}_2\text{-nfTa}_2\text{O}_5$  could absorb hydrogen at a temperature of 290 K and absorb more than 5 wt % hydrogen within 10 min at 373 K. The enthalpy values of hydrogen absorption and desorption were calculated to be  $80 \pm 2$  and  $76 \pm 3$  kJ/mol, respectively, which indicated that there is no change in thermodynamics for magnesium hydride doped by  $\text{nfTa}_2\text{O}_5$ . In summary, the  $\text{nfTa}_2\text{O}_5$  dopant can enhance the kinetics without altering the thermodynamics.

Mustafa et al. [70] reported the hydrogen storage properties of the ball-milled  $\text{MgH}_2 + 5 \text{ wt\% CeO}_2$  at a speed of 400 rpm in an argon atmosphere. The results showed that the hydrogenation rate of

CeO<sub>2</sub> doped MgH<sub>2</sub> composites was faster than pristine magnesium hydride. In addition, about 3.6 wt % hydrogen is released within 30 min for MgH<sub>2</sub> + 5 wt % CeO<sub>2</sub> composites while less than 1.0 wt % hydrogen is released for pure MgH<sub>2</sub> (Figure 10). Moreover, the activation energies of the CeO<sub>2</sub> doped MgH<sub>2</sub> composite and pure MgH<sub>2</sub> were determined to be 133.62 and 108.65 kJ/mol, respectively, which indicated that the introduction of CeO<sub>2</sub> could lead to a great improvement in hydrogen desorption. That is, the enhanced performance of hydrogen storage is due to the formation of CeH<sub>2</sub> and CeO<sub>2</sub> species.

Recently, Lin et al. [71] reported a novel method to fabricate a composite of CeH<sub>2.73</sub>/CeO<sub>2</sub> nanoparticles in Mg-based hydrides from hydrogenation and oxidation upon an amorphous Mg<sub>80</sub>Ce<sub>10</sub>Ni<sub>10</sub> alloy. Interestingly, there was a spontaneous hydrogen release effect at the CeH<sub>2.73</sub>/CeO<sub>2</sub> interface, which leads to a more dramatic increase of catalysis than either CeH<sub>2.73</sub> alone or the CeO<sub>2</sub> catalyst.

Milosevic et al. [72] fabricated two doped MgH<sub>2</sub> composites with different contents (5 and 15 wt %) of VO<sub>2</sub> with particle size in the range of 0.6–100 μm via mechanical milling. The 5 wt % VO<sub>2</sub> doped MgH<sub>2</sub> released 4.9 wt % hydrogen after about 120 s at 350 °C in the pressure of 1 bar while the other reached a capacity of 4.3 wt % after 85 s at 350 °C in the pressure of 0.7 bar for the first desorption cycle. In addition, the activation energies of desorption for MgH<sub>2</sub> + 5 wt % VO<sub>2</sub> and MgH<sub>2</sub> + 15 wt % VO<sub>2</sub> composites were 54 ± 5 and 65 ± 5 kJ/mol H<sub>2</sub>, respectively. The two values decrease significantly when compared with that of the pure MgH<sub>2</sub> (161 kJ/mol H<sub>2</sub>), suggesting fast hydrogen desorption kinetics. The improved performance may be attributed to structure defects, numbers of vacancies and the presence of VO<sub>2</sub>/VH<sub>2</sub>.

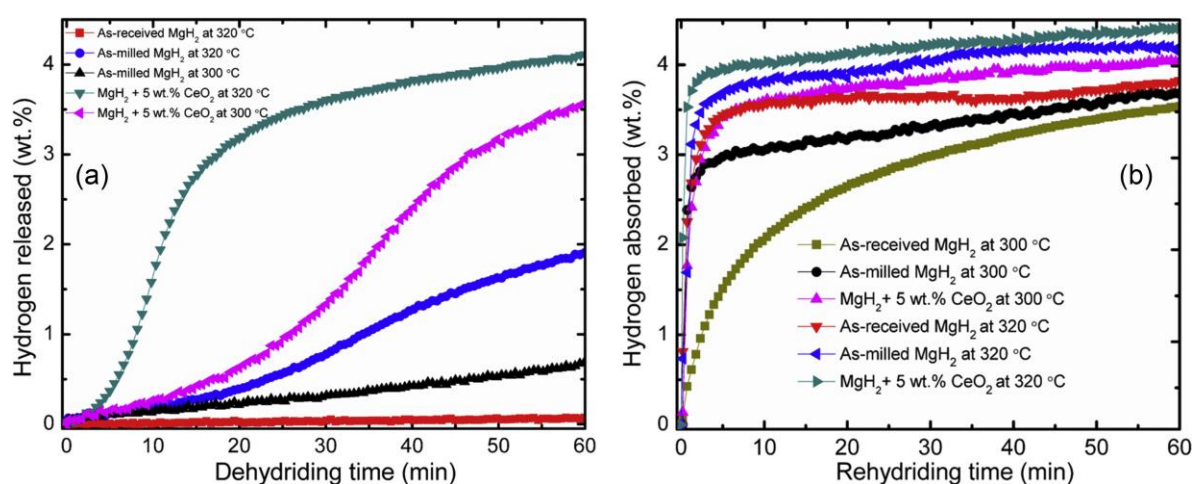


**Figure 10.** Isothermal dehydrogenation kinetics (a) and hydrogenation kinetics (b) of the as-milled MgH<sub>2</sub> and MgH<sub>2</sub> doped with 5 wt % CeO<sub>2</sub> at 320 °C and 300 °C. Adapted with permission from [70], Copyright Elsevier, 2017.

Cabo et al. [73] ball-milled a mixture of magnesium hydride and 5 wt % mesoporous oxides (Co<sub>3</sub>O<sub>4</sub>, NiCo<sub>2</sub>O<sub>4</sub> and NiO) synthesized by multi-step nano-casting at a rate of 360 rpm under an argon atmosphere for 24 h. They found that the values of desorption temperature and desorption enthalpy for the NiO-doped magnesium hydride is the lowest, followed by NiCo<sub>2</sub>O<sub>4</sub>, Co<sub>3</sub>O<sub>4</sub> and pure MgH<sub>2</sub>. When it comes to absorption/desorption rate, the introduction of NiCo<sub>2</sub>O<sub>4</sub> shows the fastest absorption rate, while the NiO-doped magnesium hydride shows the highest desorption rate.

Different metal oxides (Cr<sub>2</sub>O<sub>3</sub>, TiO<sub>2</sub>, Fe<sub>3</sub>O<sub>4</sub>, Fe<sub>2</sub>O<sub>3</sub>, In<sub>2</sub>O<sub>3</sub> and ZnO) and commercial magnesium hydride powder were ball-milled in a Uniball-5 mill for 20 h by Polanski et al. [74]. The catalytic effects of these metal oxides introduced in the magnesium hydride on the hydrogen sorption properties were also investigated. It is found that these six additives doped in magnesium hydride present various behaviors. The Cr<sub>2</sub>O<sub>3</sub> doped and TiO<sub>2</sub> doped greatly improve the hydrogenation process.

More importantly, the  $\text{Cr}_2\text{O}_3$  doped absorbed hydrogen to nearly full capacity within 2 min. The  $\text{Fe}_3\text{O}_4$  and  $\text{Fe}_2\text{O}_3$  doped showed a negligible influence while the  $\text{In}_2\text{O}_3$  and  $\text{ZnO}$  doped seem to inhibit hydrogenation. Besides, all the metal oxides studied except for  $\text{In}_2\text{O}_3$  improve the dehydrogenation properties with respect to the desorption kinetics. It is clearly seen that the  $\text{In}_2\text{O}_3$  dopant seems to inhibit the desorption reaction after 30 min when compared with the magnesium hydride without any additives. Concerning the decomposition enthalpy, the study found that this may not be affected by the introduction of metal oxide during the second cycle while it has a smaller value during the first cycle due to a high numbers of defects.

Chen et al. [75] prepared  $\text{MgH}_2$  and  $\text{ZrO}_2$  composites in molar fractions of 99:1 and 95:5 by ball milling the mixture for 20 h under the pressure of 1 atm Ar atmosphere. They found that the grain sizes range for  $\text{MgH}_2$ - $\text{ZrO}_2$  with molar ratios of 99:1 and 95:5 were 80~200 nm and 60~100 nm, respectively. Besides, the hydrogen storage capacity of  $\text{MgH}_2$  and  $\text{ZrO}_2$  composites with a molar ratio of 95:5 is 6.75 wt % at 423 K, and is still 4.0 wt % at 298 K. In addition, the activation energy for the hydrogenation reaction of  $\text{MgH}_2$ - $\text{ZrO}_2$  composites with a molar ratio of 95:5 is 13.05 kJ/mol  $\text{H}_2$ . The improved performance of as-prepared materials was attributed to the grain refining effect induced by the Zr catalyst.

In conclusion, metal oxides can be a good alternative to introduce into Mg-based materials to improve the hydrogen storage kinetics.

### 3.3. Halides Doped

It is reported that the introduction of some halides into Mg-based material can have an influence on hydrogen storage properties.

Ivanov et al. [76] investigated the effects of different inorganic salts ( $\text{NaF}$ ,  $\text{NaCl}$ ,  $\text{MgF}_2$  and  $\text{CrCl}_3$ ) ball-milled with Mg-based materials, on the hydrogenation and dehydrogenation properties. It was found that the introduction of inorganic salts not only boost the metal powdering, but also modify the metal surface. Besides, doping of different inorganic salts shows various reaction kinetics, especially for the first cycle of hydrogenation. Only the Mg- $\text{NaCl}$  composite showed a sigmoid kinetic curve at first hydriding but without an induction period contrary to other as-milled composites, which may be due to their natures.

Jin et al. [77] fabricated a series of 1~10 mol% transition metal fluorides ( $\text{NiF}_2$ ,  $\text{TiF}_3$ ,  $\text{VF}_4$ ,  $\text{NbF}_5$ ,  $\text{ZrF}_4$ ,  $\text{CrF}_2$ ,  $\text{FeF}_2$ ,  $\text{CuF}_2$ ,  $\text{CeF}_3$ ,  $\text{YF}_3$ ) doped magnesium hydride to study their hydrogenation and dehydrogenation properties. After milling for 15 min, they found that it is these hydride phases formed by the reaction between  $\text{MgH}_2$  or metal-hydrogen solid solutions that improve the hydrogenation kinetics rather than the fluorides. A similar result was also reported by Wang et al. [78] for the doping of Ti-based materials.

Danaie et al. [79] used transmission electron microscopy analysis to investigate the  $\text{TiF}_3$  doped magnesium hydride. Results showed that the catalyzed  $\text{TiF}_3$  doped magnesium hydride has excellent hydrogen storage kinetics at various temperatures. In addition, the catalyzed  $\text{TiF}_3$  doped magnesium hydride could be cycled many times with no significant degradation and both the hydride and the metal phase can be found during the absorption and desorption processes, which is very different from the pure magnesium hydride. Moreover, the number of hydride nuclei does not increase too much in the process of absorption while the introduction of  $\text{TiF}_3$  can dramatically increase the number of the newly formed magnesium crystallites. Besides, the doped  $\text{TiF}_3$  also boost extensive twinning in the hydride phase.

Lin et al. [80] ball-milled the mixture of magnesium hydride and cerium fluorides ( $\text{CeF}_3$  and  $\text{CeF}_4$ ) at the rate of 400 rpm for 4 h. It was found that the introduction of  $\text{CeF}_3$  present almost the same values of hydrogen desorption temperature and activation energy as those of the ball-milled magnesium hydride, while the doping of  $\text{CeF}_4$  decreased significantly. The reduced hydrogen desorption temperature and activation energy of  $\text{CeF}_4$  doped magnesium hydride may be due to the

easy electron transfer induced from the high valence Ce-cation and the formation of the F-containing Ce-F-Mg species on the  $\text{CeF}_4/\text{MgH}_2$  interface.

Ismail [81] used 10 wt %  $\text{LaCl}_3$  ball-milled with magnesium hydride to study the hydrogen storage properties. He found that the introduction of  $\text{LaCl}_3$  decreased the desorption temperature (50 °C less) and the activation energy of dehydrogenation (23 kJ/mol less) compared with as-milled pure magnesium hydride. When it comes to absorption and desorption kinetics, the absorption capacities for the doped and pure magnesium hydride are 5.1 wt % and 3.8 wt % in 2 min at 300 °C. Besides, 4.2 wt % hydrogen is released for the doped magnesium hydride while only 0.2 wt % for the undoped magnesium hydride. In summary, the doping of  $\text{LaCl}_3$  can enhance the kinetics of hydrogen storage due to the catalytic effect of the La-Mg alloy and the  $\text{MgCl}_2$  formed during the heating process.

A series of halide additives ( $\text{NbF}_5$ ,  $\text{NbCl}_5$ ,  $\text{TaF}_5$ ,  $\text{ZrF}_4$ ,  $\text{ZrCl}_4$ ,  $\text{CeF}_3$ ,  $\text{CdF}_2$ ,  $\text{CdCl}_2$ ,  $\text{TiCl}_3$ ,  $\text{TiF}_3$ ,  $\text{BaCl}_2$ ,  $\text{BaF}_2$ ,  $\text{NaF}$ ,  $\text{VCl}_3$ ,  $\text{FeF}_3$ ,  $\text{FeF}_2$ ,  $\text{CrCl}_2$ ,  $\text{CrF}_2$ ,  $\text{CrCl}_3$ ) doped  $\text{MgH}_2$  were investigated by Malka et al. [82]. The results showed that the magnesium hydride and halide additive composites present a strong catalytic effect on the magnesium hydride desorption process. Additionally, the fluorides exhibit a better catalytic effect when compared with chlorides, which is in agreement with the results reported by Ma et al. [83]. It was also found that the desorption temperatures for halides of higher oxidation states are much lower than that of lower oxidation states and the halides from group IV and V are the best catalysts among the studied materials.

To sum up, doping with halides can improve the kinetics by decreasing the desorption temperature and the activation energy. However, the hydrogen storage capacity is reduced owing to the introduction of the above additives which normally do not absorb hydrogen.

### 3.4. Other Additives

Besides the above-mentioned additives, some other additives have also been investigated, such as sulfide [33,84–86], and nitride [87–90]. Jia et al. [85] fabricated  $\text{MoS}_2$  and then investigated the effects of  $\text{MoS}_2$  additive on the hydrogen storage properties. It was found that the hydrogen storage capacity of  $\text{MgH}_2$  doped by  $\text{MoS}_2$  ( $\text{MgH}_2\text{-MoS}_2$ ) was 3.01 wt %, which is higher than that of pure  $\text{MgH}_2$  (1.88 wt %) under the same conditions. In addition, the hydrogen absorption/desorption for  $\text{MgH}_2\text{-MoS}_2$  was also improved. When it comes to hydrogen absorption kinetics, the uptake time for reaching 90% of the maximum hydrogen storage capacity of  $\text{MgH}_2\text{-MoS}_2$  and pure  $\text{MgH}_2$  was 72 min and 13 min, respectively. This means that the doping of  $\text{MoS}_2$  is effective in ameliorating the hydrogen absorption kinetics of  $\text{MgH}_2$ . The enhancement of hydrogen absorption and desorption kinetics was ascribed to the catalytic effect of  $\text{MgS}$  and  $\text{Mo}$  or  $\text{MgO}$  and  $\text{Mo}$ . Zhang et al. [86] ball-milled a mixture of  $\text{MgH}_2$  and 20 wt %  $\text{Fe}_3\text{S}_4$  to investigate the effects of  $\text{Fe}_3\text{S}_4$  on hydrogen storage properties. Results showed that the  $\text{MgH}_2$  added by  $\text{Fe}_3\text{S}_4$  presented three times higher hydrogen storage capacity and a two times faster hydrogen desorption rate than that of pure  $\text{MgH}_2$ . In addition, the introduction of  $\text{Fe}_3\text{S}_4$  decreased the dehydrogenation temperature by 90 K in comparison with the pure  $\text{MgH}_2$ . The improvement in hydrogen storage performance may be attributed to the catalytic effect of the new formation of  $\text{Fe}$  and  $\text{MgS}$ . Xie et al. [33] prepared flower-like  $\text{NiS}$  particles and subsequently ball-milled with  $\text{Mg}$  to study hydrogen storage behaviors. It quickly absorbed 3.5 wt % hydrogen within 10 min and desorbed 3.1 wt % hydrogen within 10 min at 573 K. The activation energies of hydrogen absorption and hydrogen desorption decreased to 45.45 and 64.71 kJ/mol, respectively. The authors thought that the enhancement of hydrogen storage properties may be attributed to the synergistic catalytic effects of the in situ formed  $\text{MgS}$ ,  $\text{Ni}$  and  $\text{Mg}_2\text{Ni}$  multiple-phase catalysts during the hydrogenation/dehydrogenation process.

Besides the introduction of sulfides, nitrides have also been added into the  $\text{Mg}/\text{MgH}_2$  system to improve the hydrogen storage performance. Different with previous discussed additives, here the nitrides contributed to hydrogen absorption/desorption capacity. Zhang and collaborators ball-milled the  $\text{MgH}_2$  and  $\text{Li}_3\text{N}$  mixture with a ratio of 1:1. They found that the  $\text{MgH}_2\text{-Li}_3\text{N}$  had a capacity of about 3.2 wt % under a pressure of 10 MPa with an onset absorption temperature of 403 K [88].



Based on their previous work, Zhang et al. [89] ball-milled different ratios of MgH<sub>2</sub> and Li<sub>3</sub>N mixture (Li<sub>3</sub>N:MgH<sub>2</sub> = 0.5, 1, 2) under the same conditions to obtain a high amount of LiMgN and study the hydrogen storage performances. It was found that the hydrogen storage capacity and dehydrogenation storage capacity were both advanced by increasing the content of Li<sub>3</sub>N. Among the three obtained samples, the MgH<sub>2</sub>-2Li<sub>3</sub>N absorbed almost 7.3 wt % hydrogen at 523 K under the hydrogen pressure of 10 MPa and released 3.3 wt % hydrogen at 623 K under 0.01 MPa. The existence of LiMgN and excess of Li<sub>3</sub>N may explain why the hydrogen storage performance of ball-milled MgH<sub>2</sub>-Li<sub>3</sub>N was improved. Wang et al. [90] fabricated the Ni<sub>3</sub>N@N-doped carbon (Ni<sub>3</sub>N@NC) with a core-shell structure and subsequently ball-milled the MgH<sub>2</sub> and as-obtained Ni<sub>3</sub>N@NC with different ratios to investigate the differences in hydrogen storage performance. Results showed that the MgH<sub>2</sub>-5 wt % Ni<sub>3</sub>N@NC composites presented the best hydrogen storage performances among the studied samples. The MgH<sub>2</sub>-5 wt % Ni<sub>3</sub>N@NC composites desorbed 6.0 wt % hydrogen (only 0.2 wt % hydrogen for the pure MgH<sub>2</sub>) within 20 min at 598 K and absorbed 6.1 wt % hydrogen within 100 s (30 min for pure MgH<sub>2</sub>) at 573 K for rehydrogenation under the same conditions. In summary based on the above-mentioned reports, the sulfides and nitrides additives introduced in the Mg/MgH<sub>2</sub> systems greatly enhanced hydrogen storage performance.

#### 4. Summary and Outlook

Hydrogen storage is a key challenge which needs to be resolved in order to move towards a hydrogen society. Mg-based materials are thought to be promising candidates owing to their many advantages, which include low price, great abundance and theoretically high hydrogenation capacity. However, poor kinetics and high desorption temperature hinder their application as hydrogen storage materials. For onboard storage, it is expected that effective Mg-based materials can be synthesized to enhance the kinetics and decrease the desorption temperature for one bar hydrogen equilibrium pressure below 100 °C. Tremendous progress in the kinetics enhancement and thermodynamic tailoring of downsized Mg/MgH<sub>2</sub> or those doped by various additives (transition metals, metal oxides, halides, etc.) has been made. The positive effect of downsizing and catalysts on kinetics is widely accepted among researchers. However, for the downsizing effect on the absorption and desorption thermodynamics of Mg-MgH<sub>2</sub>, the hydrogen storage community reports different results. We believe some of the observed thermodynamics change by plotting the van't Hoff equations at different temperatures, may be due to factors such as the different equilibrium parameters used for identifying equilibrium states and deriving equilibrium pressure values during PCT measurements, or different kinetic performance of the samples which may affect the equilibrium pressures when using the same equilibrium state parameters. Nevertheless, these developed materials are still not yet satisfactory for commercialization. Nanostructured materials appear to have some aggregation problems during cycling, and this needs to be solved. It has been reported that Mg-based materials obtained by nano-confinement, which can block grain growth and retain the nanostructure of materials, may improve the kinetics of absorption/desorption, and also may somehow change thermodynamic destabilization [8,91,92]. Emerging ideas, such as new composite materials, metastable alloys, geometrical storage materials, as well as nano-confinement technology, may give us some new directions to develop Mg-based hydrogen storage materials in the future. On the other hand, Mg-based nanomaterials combined with solid oxide fuel cells for stationary energy storage have been proposed, and this makes it possible to apply Mg-based hydrogen storage materials to large-scale storage with a working temperature for storage materials higher than 250 °C [43]. In this case, thermodynamic change is no longer a problem.

**Acknowledgments:** H.S. acknowledges the Macau Science and Technology Development Fund (FDCT) for funding (project no. 118/2016/A3), and this work was also partially supported by a Start-Up Research Fund from the University of Macau (SRG2016-00088-FST). H.L. is also thankful for the support of the National Natural Science Foundation of China (no. 51601090).

**Author Contributions:** H.S. conceived and designed the concept. H.L. designed some of the main ideas for the construction of the paper construction. J.L., B.L. and W.L. contributed to the writing.

**Conflicts of Interest:** The authors declare no conflict of interest.

## References

1. Zhu, M.; Lu, Y.; Ouyang, L.; Wang, H. Thermodynamic tuning of Mg-based hydrogen storage alloys: A review. *Materials* **2013**, *6*, 4654–4674. [[CrossRef](#)] [[PubMed](#)]
2. Shao, H.; He, L.; Lin, H.; Li, H.-W. Progress and trends in magnesium-based materials for energy-storage research: A review. *Energy Technol.* **2018**. [[CrossRef](#)]
3. Trimm, D.; Önsan, Z.I. Onboard fuel conversion for hydrogen-fuel-cell-driven vehicles. *Catal. Rev.* **2001**, *43*, 31–84. [[CrossRef](#)]
4. Singh, S.; Jain, S.; Venkateswaran, P.S.; Tiwari, A.K.; Nouni, M.R.; Pandey, J.K.; Goel, S. Hydrogen: A sustainable fuel for future of the transport sector. *Renew. Sustain. Energy Rev.* **2015**, *51*, 623–633. [[CrossRef](#)]
5. Sakintuna, B.; Lamari-Darkrim, F.; Hirscher, M. Metal hydride materials for solid hydrogen storage: A review. *Int. J. Hydrog. Energy* **2007**, *32*, 1121–1140. [[CrossRef](#)]
6. Jain, I.P. Hydrogen the fuel for 21st century. *Int. J. Hydrog. Energy* **2009**, *34*, 7368–7378. [[CrossRef](#)]
7. Hudson, M.S.L.; Pukazhselvan, D.; Sheeja, G.I.; Srivastava, O.N. Studies on synthesis and dehydrogenation behavior of magnesium alanate and magnesium–sodium alanate mixture. *Int. J. Hydrog. Energy* **2007**, *32*, 4933–4938.
8. Sadhasivama, T.; Kimb, H.; Jungc, S.; Rohd, S.; Parka, J.; Junga, H. Dimensional effects of nanostructured Mg/MgH<sub>2</sub> for hydrogen storage applications: A review. *Renew. Sustain. Energy Rev.* **2017**, *72*, 523–534. [[CrossRef](#)]
9. Sandí, G. Hydrogen storage and its limitations. *Electrochem. Soc. Interface* **2004**, *13*, 40–44.
10. Züttel, A. Hydrogen storage methods. *Naturwissenschaften* **2004**, *91*, 157–172. [[CrossRef](#)] [[PubMed](#)]
11. Schlapbach, L.; Züttel, A. Hydrogen-storage materials for mobile applications. *Nature* **2001**, *414*, 353–358. [[CrossRef](#)] [[PubMed](#)]
12. Xia, G.; Tan, Y.; Chen, X.; Sun, D.; Guo, Z.; Liu, H.; Ouyang, L.; Zhu, M.; Yu, X. Monodisperse magnesium hydride nanoparticles uniformly self-assembled on graphene. *Adv. Mater.* **2015**, *27*, 5981–5988. [[CrossRef](#)] [[PubMed](#)]
13. Orimo, S.; Nakamori, Y.; Eliseo, J.R.; Zuttel, A.; Jensen, C.M. Complex hydrides for hydrogen storage. *Chem. Rev.* **2007**, *107*, 4111–4132. [[CrossRef](#)] [[PubMed](#)]
14. Wan, L.F.; Liu, Y.; Cho, E.S.; Forster, J.D.; Jeong, S.; Wang, H.; Urban, J.J.; Guo, J.; Prendergast, D. Atomically thin interfacial suboxide key to hydrogen storage performance enhancements of magnesium nanoparticles encapsulated in reduced graphene oxide. *Nano Lett.* **2017**, *17*, 5540–5545. [[CrossRef](#)] [[PubMed](#)]
15. Cho, E.S.; Ruminski, A.M.; Aloni, S.; Liu, Y.; Guo, J.; Urban, J.J. Graphene oxide/metal nanocrystal multilaminates as the atomic limit for safe and selective hydrogen storage. *Nat. Commun.* **2016**, *7*, 10804. [[CrossRef](#)] [[PubMed](#)]
16. Zhang, H.; Zheng, X.; Tian, X.; Liu, Y.; Li, X. New approaches for rare earth-magnesium based hydrogen storage alloys. *Prog. Nat. Sci. Mater. Int.* **2017**, *27*, 50–57. [[CrossRef](#)]
17. Wang, H.; Lin, H.; Cai, W.; Ouyang, L.; Zhu, M. Tuning kinetics and thermodynamics of hydrogen storage in light metal element based systems—A review of recent progress. *J. Alloy. Compd.* **2016**, *658*, 280–300. [[CrossRef](#)]
18. Li, L.; Peng, B.; Ji, W.; Chen, J. Studies on the hydrogen storage of magnesium nanowires by density functional theory. *J. Phys. Chem. C* **2009**, *113*, 3007–3013. [[CrossRef](#)]
19. Wagemans, R.W.P.; van Lenthe, J.H.; de Jongh, P.E.; van Dillen, A.J.; Jong, K.P.D. Hydrogen storage in magnesium clusters quantum chemical study. *J. Am. Chem. Soc.* **2005**, *127*, 16675–16680. [[CrossRef](#)] [[PubMed](#)]
20. Lu, J.; Choi, Y.J.; Fang, Z.Z.; Sohn, H.Y.; Ronnebro, E. Hydrogen storage properties of nanosized MgH<sub>2</sub>–0.1TiH<sub>2</sub> prepared by ultrahigh-energy–high-pressure milling. *J. Am. Chem. Soc.* **2009**, *131*, 15843–15852. [[CrossRef](#)] [[PubMed](#)]

21. Shao, H.; Felderhoff, M.; Schuth, F. Hydrogen storage properties of nanostructured MgH<sub>2</sub>/TiH<sub>2</sub> composite prepared by ball milling under high hydrogen pressure. *Int. J. Hydrog. Energy* **2011**, *36*, 10828–10833. [[CrossRef](#)]
22. Li, W.; Li, C.; Ma, H.; Chen, J. Magnesium nanowires enhanced kinetics for hydrogen absorption and desorption. *J. Am. Chem. Soc.* **2007**, *129*, 6710–6711. [[CrossRef](#)] [[PubMed](#)]
23. Zaluska, A.; Zaluski, L.; Ström-Olsen, J.O. Structure, catalysis and atomic reactions on the nano-scale a systematic approach to metal hydrides for hydrogen storage. *Appl. Phys. A Mater. Sci. Process.* **2001**, *72*, 157–165. [[CrossRef](#)]
24. Cheung, S.; Deng, W.; van Duin, A.C.T.; Goddard, W.A. Reaxffmgh reactive force field for magnesium hydride systems. *J. Phys. Chem. A* **2005**, *109*, 851–859. [[CrossRef](#)] [[PubMed](#)]
25. Gross, A.F.; Ahn, C.C.; van Atta, S.L.; Liu, P.; Vajo, J.J. Fabrication and hydrogen sorption behaviour of nanoparticulate MgH<sub>2</sub> incorporated in a porous carbon host. *Nanotechnology* **2009**, *20*, 204005. [[CrossRef](#)] [[PubMed](#)]
26. Lin, H.; Zhang, C.; Wang, H.; Ouyang, L.; Zhu, Y.; Li, L.; Wang, W.; Zhu, M. Controlling nanocrystallization and hydrogen storage property of Mg-based amorphous alloy via a gas-solid reaction. *J. Alloy. Compd.* **2016**, *685*, 272–277. [[CrossRef](#)]
27. Shao, H.; Wang, Y.; Xu, H.; Li, X. Hydrogen storage properties of magnesium ultrafine particles prepared by hydrogen plasma-metal reaction. *Mater. Sci. Eng. B* **2004**, *110*, 221–226. [[CrossRef](#)]
28. Shao, H.; Xu, H.; Wang, Y.; Li, X. Preparation and hydrogen storage properties of Mg<sub>2</sub>Ni intermetallic nanoparticles. *Nanotechnology* **2004**, *15*, 269–274. [[CrossRef](#)]
29. Shao, H.; Felderhoff, M.; Schuth, F.; Weidenthaler, C. Nanostructured Ti-catalyzed MgH<sub>2</sub> for hydrogen storage. *Nanotechnology* **2011**, *22*, 235401. [[CrossRef](#)] [[PubMed](#)]
30. Sun, Y.; Shen, C.; Lai, Q.; Liu, W.; Wang, D.; Aguey-Zinsou, K.-F. Tailoring magnesium based materials for hydrogen storage through synthesis: Current state of the art. *Energy Storage Mater.* **2018**, *10*, 168–198. [[CrossRef](#)]
31. Shao, H.; Felderhoff, M.; Weidenthaler, C. Kinetics enhancement, reaction pathway change, and mechanism clarification in LiBH<sub>4</sub> with Ti-catalyzed nanocrystalline MgH<sub>2</sub> composite. *J. Phys. Chem. C* **2015**, *119*, 2341–2348.
32. Stampfer, J.F.; Holley, J.R.C.E.; Suttle, J.J.F. The magnesium-hydrogen system 1–3. *J. Am. Chem. Soc.* **1960**, *82*, 3504–3508. [[CrossRef](#)]
33. Xie, X.; Ma, X.; Liu, P.; Shang, J.; Li, X.; Liu, T. Formation of multiple-phase catalysts for the hydrogen storage of mg nanoparticles by adding flowerlike NiS. *ACS Appl. Mater. Interfaces* **2017**, *9*, 5937–5946. [[CrossRef](#)] [[PubMed](#)]
34. Pedersen, A.S.; Kjoller, J.; Larsen, B.; Vigeholm, B. Magnesium for hydrogen storage. *Int. J. Hydrog. Energy* **1983**, *8*, 205–211. [[CrossRef](#)]
35. Konarova, M.; Tanksale, A.; Beltramini, J.N.; Lu, G.Q. Effects of nano-confinement on the hydrogen desorption properties of MgH<sub>2</sub>. *Nano Energy* **2013**, *2*, 98–104. [[CrossRef](#)]
36. Kumar, S.; Tiwari, G.P. Thermodynamics and kinetics of MgH<sub>2</sub>-nfta<sub>2</sub>O<sub>5</sub> composite for reversible hydrogen storage application. *J. Mater. Sci.* **2017**, *52*, 6962–6968. [[CrossRef](#)]
37. Cho, E.S.; Ruminski, A.M.; Liu, Y.; Shea, P.T.; Kang, S.; Zaia, E.W.; Park, J.Y.; Chuang, Y.; Yuk, J.M.; Zhou, X.; et al. Hierarchically controlled inside-out doping of Mg nanocomposites for moderate temperature hydrogen storage. *Adv. Funct. Mater.* **2017**, *27*. [[CrossRef](#)]
38. Li, Y.; Liu, Y.; Zhang, X.; Zhou, D.; Lu, Y.; Gao, M.; Pan, H. An ultrasound-assisted wet-chemistry approach towards uniform Mg(BH<sub>4</sub>)<sub>2</sub>·6NH<sub>3</sub> nanoparticles with improved dehydrogenation properties. *J. Mater. Chem. A* **2016**, *4*, 8366–8373. [[CrossRef](#)]
39. Baldé, C.P.; Hereijgers, B.P.C.; Bitter, J.H.; Jong, K.P.D. Sodium alanate nanoparticles—Linking size to hydrogen storage properties. *J. Am. Chem. Soc.* **2008**, *130*, 6761–6765. [[CrossRef](#)] [[PubMed](#)]
40. Pang, Y.; Liu, Y.; Gao, M.; Ouyang, L.; Liu, J.; Wang, H.; Zhu, M.; Pan, H. A mechanical-force-driven physical vapour deposition approach to fabricating complex hydride nanostructures. *Nat. Commun.* **2014**, *5*, 3519. [[CrossRef](#)] [[PubMed](#)]
41. Norberg, N.S.; Arthur, T.S.; Fredrick, S.J.; Prieto, A.L. Size-dependent hydrogen storage properties of Mg nanocrystals prepared from solution. *J. Am. Chem. Soc.* **2011**, *133*, 10679–10681. [[CrossRef](#)] [[PubMed](#)]

42. Bérubé, V.; Radtke, G.; Dresselhaus, M.; Chen, G. Size effects on the hydrogen storage properties of nanostructured metal hydrides: A review. *Int. J. Energy Res.* **2007**, *31*, 637–663. [[CrossRef](#)]
43. Shao, H. Heat modeling and material development of Mg-based nanomaterials combined with solid oxide fuel cell for stationary energy storage. *Energies* **2017**, *10*, 1767. [[CrossRef](#)]
44. Shao, H.; Ma, W.; Kohno, M.; Takata, Y.; Xin, G.; Fujikawa, S.; Fujino, S.; Bishop, S.; Li, X. Hydrogen storage and thermal conductivity properties of Mg-based materials with different structures. *Int. J. Hydrog. Energy* **2014**, *39*, 9893–9898. [[CrossRef](#)]
45. Shao, H.; Asano, K.; Enoki, H.; Akiba, E. Fabrication, hydrogen storage properties and mechanistic study of nanostructured Mg<sub>50</sub>Co<sub>50</sub> body-centered cubic alloy. *Scr. Mater.* **2009**, *60*, 818–821. [[CrossRef](#)]
46. Wang, Y.; Wang, Y. Recent advances in additive-enhanced magnesium hydride for hydrogen storage. *Prog. Nat. Sci. Mater. Int.* **2017**, *27*, 41–49. [[CrossRef](#)]
47. Crivello, J.-C.; Denys, R.V.; Dornheim, M.; Felderhoff, M.; Grant, D.M.; Huot, J.; Jensen, T.R.; de Jongh, P.; Lacroche, M.; Walker, G.S.; et al. Mg-based compounds for hydrogen and energy storage. *Appl. Phys. A* **2016**, *122*, 1–17. [[CrossRef](#)]
48. Webb, C.J. A review of catalyst-enhanced magnesium hydride as a hydrogen storage material. *J. Phys. Chem. Solids* **2015**, *84*, 96–106. [[CrossRef](#)]
49. Hanada, N.; Ichikawa, T.; Fujii, H. Catalytic effect of nanoparticle 3d-transition metals on hydrogen storage properties in magnesium hydride MgH<sub>2</sub> prepared by mechanical milling. *J. Phys. Chem. B* **2005**, *109*, 7188–7194. [[CrossRef](#)] [[PubMed](#)]
50. Liang, G.; Huot, J.; Boily, S.; van Neste, A.; Schulz, R. Catalytic effect of transition metals on hydrogen sorption in nanocrystalline ball milled MgH<sub>2</sub>-Tm (Tm = Ti, V, Mn, Fe and Ni). *J. Alloy. Compd.* **1999**, *292*, 247–252. [[CrossRef](#)]
51. Liang, G.; Huot, J.; Boily, S.; Schulz, R. Hydrogen desorption kinetics of a mechanically milled MgH<sub>2</sub>+5at.%v nanocomposite. *J. Alloy. Compd.* **2000**, *305*, 239–245. [[CrossRef](#)]
52. Cui, J.; Wang, H.; Liu, J.; Ouyang, L.; Zhang, Q.; Sun, D.; Yao, X.; Zhu, M. Remarkable enhancement in dehydrogenation of MgH<sub>2</sub> by a nano-coating of multi-valence Ti-based catalysts. *J. Mater. Chem. A* **2013**, *1*, 5603–5611. [[CrossRef](#)]
53. Lu, C.; Zou, J.; Zeng, X.; Ding, W. Hydrogen storage properties of core-shell structured Mg@TM (TM = Co, V) composites. *Int. J. Hydrog. Energy* **2017**, *42*, 15246–15255. [[CrossRef](#)]
54. Zou, J.; Guo, H.; Zeng, X.; Zhou, S.; Chen, X.; Ding, W. Hydrogen storage properties of Mg-Tm-La (Tm = Ti, Fe, Ni) ternary composite powders prepared through arc plasma method. *Int. J. Hydrog. Energy* **2013**, *38*, 8852–8862. [[CrossRef](#)]
55. Yu, H.; Bennici, S.; Auroux, A. Hydrogen storage and release: Kinetic and thermodynamic studies of MgH<sub>2</sub> activated by transition metal nanoparticles. *Int. J. Hydrog. Energy* **2014**, *39*, 11633–11641. [[CrossRef](#)]
56. Kuji, T.; Nakayama, S.; Hanzawa, N.; Tabira, Y. Synthesis of nano-structured b.c.c. Mg-Tm-V (Tm = Ni, Co, Cu) alloys and their hydrogen solubility. *J. Alloy. Compd.* **2003**, *356–357*, 456–460. [[CrossRef](#)]
57. Xie, L.; Liu, Y.; Zhang, X.; Qu, J.; Wang, Y.; Li, X. Catalytic effect of Ni nanoparticles on the desorption kinetics of MgH<sub>2</sub> nanoparticles. *J. Alloy. Compd.* **2009**, *482*, 388–392. [[CrossRef](#)]
58. Kalinichenka, S.; Rontzsch, L.; Kieback, B. Structural and hydrogen storage properties of melt-spun Mg-Ni-Y alloys. *Int. J. Hydrog. Energy* **2009**, *34*, 7749–7755. [[CrossRef](#)]
59. Shao, H.; Matsuda, J.; Li, H.; Akiba, E.; Jain, A.; Ichikawa, T.; Kojima, Y. Phase and morphology evolution study of ball milled Mg-Co hydrogen storage alloys. *Int. J. Hydrog. Energy* **2013**, *38*, 7070–7076. [[CrossRef](#)]
60. Shao, H.; Liu, T.; Li, X.; Zhang, L. Preparation of Mg<sub>2</sub>Ni intermetallic compound from nanoparticles. *Scr. Mater.* **2003**, *49*, 595–599. [[CrossRef](#)]
61. Shao, H.; Xu, H.; Wang, Y.; Li, X. Synthesis and hydrogen storage behavior of Mg-Co-H system at nanometer scale. *J. Solid State Chem.* **2004**, *177*, 3626–3632. [[CrossRef](#)]
62. Shao, H.; Wang, Y.; Xu, H.; Li, X. Preparation and hydrogen storage properties of nanostructured Mg<sub>2</sub>Cu alloy. *J. Solid State Chem.* **2005**, *178*, 2211–2217. [[CrossRef](#)]
63. Shao, H.; Asano, K.; Enoki, H.; Akiba, E. Preparation and hydrogen storage properties of nanostructured Mg-Ni BCC alloys. *J. Alloy. Compd.* **2009**, *477*, 301–306. [[CrossRef](#)]
64. Zhang, J.; Zhu, Y.; Lin, H.; Liu, Y.; Zhang, Y.; Li, S.; Ma, Z.; Li, L. Metal hydride nanoparticles with ultrahigh structural stability and hydrogen storage activity derived from microencapsulated nanoconfinement. *Adv. Mater.* **2017**, *29*. [[CrossRef](#)] [[PubMed](#)]

65. Oelerich, W.; Klassen, T.; Bormann, R. Metal oxides as catalysts for improved hydrogen sorption in nanocrystalline Mg-based materials. *J. Alloy. Compd.* **2001**, *315*, 237–242. [[CrossRef](#)]
66. Barkhordarian, G.; Klassen, T.; Bormann, R. Fast hydrogen sorption kinetics of nanocrystalline Mg using Nb<sub>2</sub>O<sub>5</sub> as catalyst. *Scr. Mater.* **2003**, *49*, 213–217. [[CrossRef](#)]
67. Hanada, N.; Ichikawa, T.; Hino, S.; Fujii, H. Remarkable improvement of hydrogen sorption kinetics in magnesium catalyzed with Nb<sub>2</sub>O<sub>5</sub>. *J. Alloy. Compd.* **2006**, *420*, 46–49. [[CrossRef](#)]
68. Aguey-Zinsou, K.-F.; Fernandez, J.R.A.; Klassen, T.; Bormann, R. Effect of Nb<sub>2</sub>O<sub>5</sub> on MgH<sub>2</sub> properties during mechanical milling. *Int. J. Hydrog. Energy* **2007**, *32*, 2400–2407. [[CrossRef](#)]
69. Da Conceição, M.O.T.; Brum, M.C.; Santos, D.S.D.; Dias, M.L. Hydrogen sorption enhancement by Nb<sub>2</sub>O<sub>5</sub> and Nb catalysts combined with MgH<sub>2</sub>. *J. Alloy. Compd.* **2013**, *550*, 179–184. [[CrossRef](#)]
70. Mustafa, N.S.; Ismail, M. Hydrogen sorption improvement of MgH<sub>2</sub> catalyzed by CeO<sub>2</sub> nanopowder. *J. Alloy. Compd.* **2017**, *695*, 2532–2538. [[CrossRef](#)]
71. Lin, H.; Tang, J.; Yu, Q.; Wang, H.; Ouyang, L.; Zhao, Y.; Liu, J.; Wang, W.; Zhu, M. Symbiotic CeH<sub>2.73</sub>/CeO<sub>2</sub> catalyst: A novel hydrogen pump. *Nano Energy* **2014**, *9*, 80–87. [[CrossRef](#)]
72. Sevic, S.M.; Kurko, S.; Pasquini, L.; Matovic, L.; Vujasin, R.; Novakovic, N.; Novakovic, J.G. Fast hydrogen sorption from MgH<sub>2</sub>-VO<sub>2</sub> (b) composite materials. *J. Power Sources* **2016**, *307*, 481–488.
73. Cabo, M.; Garroni, S.; Pellicer, E.; Milanese, C.; Girella, A.; Marini, A.; Rossinyol, E.; Surinach, S.; Baro, M.D. Hydrogen sorption performance of MgH<sub>2</sub> doped with mesoporous nickel- and cobalt-based oxides. *Int. J. Hydrog. Energy* **2011**, *36*, 5400–5410. [[CrossRef](#)]
74. Polanski, M.; Bystrzycki, J. Comparative studies of the influence of different nano-sized metal oxides on the hydrogen sorption properties of magnesium hydride. *J. Alloy. Compd.* **2009**, *486*, 697–701. [[CrossRef](#)]
75. Chen, B.; Chuang, Y.; Chen, C.O.-K. Improving the hydrogenation properties of MgH<sub>2</sub> at room temperature by doping with nano-size ZrO<sub>2</sub> catalyst. *J. Alloy. Compd.* **2016**, *655*, 21–27. [[CrossRef](#)]
76. Ivanov, E.; Konstanchuk, I.; Bokhonov, B.; Boldyrev, V. Hydrogen interaction with mechanically alloyed magnesium-salt composite materials. *J. Alloy. Compd.* **2003**, *359*, 320–325. [[CrossRef](#)]
77. Jin, S.; Shim, J.; Cho, Y.W.; Yi, K.-W. Dehydrogenation and hydrogenation characteristics of MgH<sub>2</sub> with transition metal fluorides. *J. Power Sources* **2007**, *172*, 859–862. [[CrossRef](#)]
78. Wang, Y.; Zhang, Q.; Wang, Y.; Jiao, L.; Yuan, H. Catalytic effects of different Ti-based materials on dehydrogenation performances of MgH<sub>2</sub>. *J. Alloy. Compd.* **2015**, *645*, S509–S512. [[CrossRef](#)]
79. Danaie, M.; Mitlin, D. TEM analysis of the microstructure in TiF<sub>3</sub>-catalyzed and pure MgH<sub>2</sub> during the hydrogen storage cycling. *Acta Mater.* **2012**, *60*, 6441–6456. [[CrossRef](#)]
80. Lin, H.; Matsuda, J.; Li, H.; Zhu, M.; Akiba, E. Enhanced hydrogen desorption property of MgH<sub>2</sub> with the addition of cerium fluorides. *J. Alloy. Compd.* **2015**, *645*, S392–S396. [[CrossRef](#)]
81. Ismail, M. Effect of LaCl<sub>3</sub> addition on the hydrogen storage properties of MgH<sub>2</sub>. *Energy* **2015**, *79*, 177–182. [[CrossRef](#)]
82. Malka, I.E.; Czujko, T.; Bystrzycki, J. Catalytic effect of halide additives ball milled with magnesium hydride. *Int. J. Hydrog. Energy* **2010**, *35*, 1706–1712. [[CrossRef](#)]
83. Ma, L.; Wang, P.; Cheng, H.-M. Hydrogen sorption kinetics of MgH<sub>2</sub> catalyzed with titanium compounds. *Int. J. Hydrog. Energy* **2010**, *35*, 3046–3050. [[CrossRef](#)]
84. Putungan, D.B.; Lin, S.; Wei, C.; Kuo, J.-L. Li adsorption, hydrogen storage and dissociation using monolayer MoS<sub>2</sub>: An ab initio random structure searching approach. *Phys. Chem. Chem. Phys.* **2015**, *17*, 11367–11374. [[CrossRef](#)] [[PubMed](#)]
85. Jia, Y.; Han, S.; Zhang, W.; Zhao, X.; Sun, P.; Liu, Y.; Shi, H.; Wang, J. Hydrogen absorption and desorption kinetics of MgH<sub>2</sub> catalyzed by MoS<sub>2</sub> and MoO<sub>2</sub>. *Int. J. Hydrog. Energy* **2013**, *38*, 2352–2356. [[CrossRef](#)]
86. Zhang, B.; Li, W.; Lv, Y.; Yan, Y.; Wu, Y. The hydrogen storage properties of MgH<sub>2</sub>-Fe<sub>3</sub>S<sub>4</sub> composites. *Energy* **2015**, *93*, 625–630. [[CrossRef](#)]
87. Hashmi, A.; Farooq, M.U.; Khan, I.; Son, J.; Hong, J. Ultra-high capacity hydrogen storage in a Li decorated two-dimensional C<sub>2</sub>N layer. *J. Mater. Chem. A* **2017**, *5*, 2821–2828. [[CrossRef](#)]
88. Zhang, B.; Wu, Y. Effects of additives on the microstructure and hydrogen storage properties of the Li<sub>3</sub>N-MgH mixture. *J. Alloy. Compd.* **2014**, *613*, 199–203. [[CrossRef](#)]
89. Zhang, B.; Li, W.; Lv, Y.; Yan, Y.; Wu, Y. Hydrogen storage properties of the mixtures MgH<sub>2</sub>-Li<sub>3</sub>N with different molar ratios. *J. Alloy. Compd.* **2015**, *645*, S464–S467. [[CrossRef](#)]

90. Zhang, Q.; Wang, Y.; Zang, L.; Chang, X.; Jiao, L.; Yuan, H.; Wang, Y. Core-shell Ni<sub>3</sub>N@nitrogen-doped carbon: Synthesis and application in MgH<sub>2</sub>. *J. Alloy. Compd.* **2017**, *703*, 381–388. [[CrossRef](#)]
91. Zhao-Karger, Z.; Hu, J.; Roth, A.; Wang, D.; Kubel, C.; Lohstroh, W.; Fichtner, M. Altered thermodynamic and kinetic properties of MgH<sub>2</sub> infiltrated in microporous scaffold. *Chem. Commun.* **2010**, *46*, 8353–8355. [[CrossRef](#)] [[PubMed](#)]
92. Jia, Y.; Sun, C.; Cheng, L.; Wahab, M.A.; Cui, J.; Zou, J.; Zhu, M.; Yao, X. Destabilization of Mg-H bonding through nano-interfacial confinement by unsaturated carbon for hydrogen desorption from MgH<sub>2</sub>. *Phys. Chem. Chem. Phys.* **2013**, *15*, 5814–5820. [[CrossRef](#)] [[PubMed](#)]



© 2018 by the authors. Licensee MDPI, Basel, Switzerland. This article is an open access article distributed under the terms and conditions of the Creative Commons Attribution (CC BY) license (<http://creativecommons.org/licenses/by/4.0/>).